HHS Public Access

Author manuscript

Immunity. Author manuscript; available in PMC 2023 November 08.

Published in final edited form as:

Immunity. 2022 November 08; 55(11): 2118–2134.e6. doi:10.1016/j.immuni.2022.08.017.

Mucosal Plasma Cells are Required to Protect the Upper Airway and Brain from Infection

Sebastian A. Wellford[1], **Annie Park Moseman**[1], **Kianna Dao**[1], **Katherine E. Wright**[1], **Allison Chen**[1], **Jona E. Plevin**[1], **Tzu-Chieh Liao**[1], **Naren Mehta**[1], **E. Ashley Moseman**[1,2,*]

[1]Department of Immunology, Duke University School of Medicine, Durham, NC, USA

[2]Lead Contact

Summary

While blood antibodies mediate protective immunity in most organs, whether they protect nasal surfaces in the upper airway is unclear. Using multiple viral infection models in mice, we found that blood-borne antibodies could not defend the olfactory epithelium. Despite high serum antibody titers, pathogens infected nasal turbinates, and neurotropic microbes invaded the brain. Using passive antibody transfers and parabiosis, we identified a restrictive blood-endothelial barrier that excluded circulating antibodies from the olfactory mucosa. Plasma cell depletions demonstrated that plasma cells must reside within olfactory tissue to achieve sterilizing immunity. Antibody blockade and genetically-deficient models revealed that this local immunity required $CD4^+$ T cells and CXCR3. Many vaccine adjuvants failed to generate olfactory plasma cells, but mucosal immunizations established humoral protection of the olfactory surface. Our identification of a blood-olfactory barrier and the requirement for tissue derived antibody has implications for vaccinology, respiratory and CNS pathogen transmission, and B-cell fate decisions.

eTOC blurb

Whether circulating antibodies protect the nasal airway from infection is unclear. Wellford et al. show that the olfactory mucosa exists outside the reach of serum antibody due to the presence of a blood-olfactory barrier. Instead, mucosal plasma cells can be recruited to protect the upper airway and brain from infection.

*Correspondence: ashley.moseman@duke.edu.

Author Contributions

S.A.W. designed, performed, and anlyzed experiments, contributed to project design and data interpretation, and wrote the manuscript. A.P.M., K.D., K.E.W., A.C., J.P., T.L., and N.M. performed and analyzed experiments. E.A.M. directed the project, designed and performed experiments, contributed to project design and data interpretation, and contributed to manuscript writing.

Declaration of Interests

The authors declare no competing interests.

Keywords

brain barriers; mucosal immunology; olfactory epithelium; B cells; adjuvants; respiratory viruses; upper respiratory tract; neurotropic pathogens; humoral immunity

Introduction

Airborne pathogens typically initiate infection in the upper respiratory tract (URT) (Bosch et al., 2013), whereas most serious complications arise from life-threatening lung damage and immunopathology (Busse, 1991). As a result, therapeutic approaches focus on protecting pulmonary function. Indeed, SARS-CoV-2 vaccines are highly effective at reducing lung viral titer (van Doremalen et al., 2020), reducing severe cases and improving overall survival (Baden et al., 2021; Polack et al., 2020).

However, vaccines for airborne pathogens should also protect the URT. Failing to impose sterilizing immunity in the nasal cavity allows for reinfection and continued disease transmission. It is unknown whether SARS-CoV-2 vaccines, or vaccines generally, provide adequate URT protection (Corbett et al., 2021; Fröberg et al., 2021; Horiuchi et al., 2021; McMahan et al., 2021). Widespread “breakthrough” SARS-CoV-2 infections in vaccinated individuals, typically with mild URT symptoms, indicate incomplete URT immunity (Bergwerk et al., 2021). Conflicting evidence obfuscates the relative importance of vaccine-induced systemic antibodies or tissue-specific immune mechanisms, such as secretory IgA, in URT mucosal surface protection (Bricker et al., 2020; Case et al., 2020; Hassan et al., 2020; Subbarao et al., 2004; van Doremalen et al., 2020; Zhou et al., 2021).

Understanding URT immunity requires appreciation of its heterogeneity. The nasal airway is composed of two juxtaposed regions: respiratory epithelium (RE) and olfactory epithelium (OE). While RE facilitates air passage into the lungs, the primary OE function is to communicate environmental odorant information for the sense of smell (Barrios et al., 2014; Chen et al., 2014a). From within the OE, olfactory sensory neurons (OSNs) project sensory dendrites into the airway and relay scent information through axon tracks that tunnel through the olfactory mucosa (OM) directly into the olfactory bulb (OB) of the brain (Figure 1a). This unique anatomy creates a single-cell pathway that pathogens exploit to bypass conventional CNS barriers (Dando et al., 2014), making olfactory protection critical for defense against neurotropic airborne pathogens.

Numerous pathogens invade the OM; while some, such as the large eukaryote *Naegleria fowleri*, migrate along olfactory axon tracts to cause fatal meningoencephalitis in the brain (Moseman, 2020), viruses such as Influenza A and B (Aronsson et al., 2003; Dumm et al., 2020), infect neurons directly. Pandemic avian influenza strains have neurotropic predilections and can infect OSNs, leading to lethal disease in animal models (Plourde et al., 2012; Schrauwen et al., 2012; van den Brand et al., 2012) and CNS disease and long-term neurologic dysfunction in humans (Jang et al., 2009; Lee et al., 2010; McCullers et al., 1999; Newland et al., 2003; Popescu et al., 2017; Reyes et al., 2019; Steininger et al., 2003). SARS-CoV-2 infects both RE and OE, as evidenced by millions of people with transient or long-term post-viral olfactory dysfunction (Brann et al., 2020; de Melo et

al., 2021; Meng et al., 2020; Renaud et al., 2021) with serious quality of life impacts for anosmic individuals (Hura et al., 2020; Xydakis et al., 2021). SARS-CoV-2 is aggressively neuroinvasive in certain animal models (Fumagalli et al., 2021; Zheng et al., 2020), and cognitive sequelae are not uncommon (Ceban et al., 2022; Premraj et al., 2022), though evidence for neuroinvasion in humans is lacking (Bauer et al., 2022; Butowt et al., 2021; de Melo et al., 2021; Khan et al., 2021).

One cytopathic rhabdovirus that hijacks the olfactory pathway to invade the CNS is vesicular stomatitis virus (VSV) (Reiss et al., 1998). VSV infection elicits a prototypically robust neutralizing antibody (nAb) response, leading to long-term immunity from reinfection (Kalinke et al., 1996; Zhou et al., 2007). Following inhalation, VSV infects OSNs and rapidly replicates in OSNs, reaching the OB within 24 hours. Although it can cause paralysis and death, VSV is typically cleared from the brain in a T cell-dependent manner ~8 days following infection (Moseman et al., 2020). Subcutaneous or intraperitoneal VSV challenge does not lead to olfactory or CNS replication, but VSV instead replicates briefly within specialized lymphoid sinus-lining macrophages (Iannacone et al., 2010). VSV's olfactory neuroinvasive ability, robust nAb generation, and capacity to infect via multiple routes make it well-suited for investigations of URT antibody protection.

Here, we showed that circulating nAbs were unable to protect the OM and brain from airway viral infection. Systemic antibody was prevented from accessing olfactory tissue by a blood-olfactory barrier. Instead, we found that local antibody secretion by extravascular plasma cells within the OM was required to protect the mucosa and brain. These tissue-resident plasma cells were recruited in a CXCR3-dependent process that relies on T cell help. Vaccine strategies using common adjuvants such as alum did not sufficiently drive OMP protection. However, vaccination strategies with a mucosal adjuvant (dmLT), and potentially mRNA vaccines, could generate olfactory plasma cells to protect the URT and CNS.

Results

Circulating antibody does not protect the olfactory mucosa from viral infection

To examine URT adaptive immune responses, we infected mice with VSV, Indiana strain (VSV or VSV-IND) via intranasal (IN) or intraperitoneal (IP) routes of infection. In naïve mice, IN VSV infection led to widespread replication in the olfactory mucosa (OM), while previously infected mice were completely protected from reinfection regardless of primary infection route (Figure 1b). OM infection also resulted in CNS neuroinvasion via olfactory nerves in naïve mice; this was prevented in immune animals (Figure 1c). IP infection did not lead to viral OM infection (Figure S1b), but both IP and IN routes of infection generated high nAb titers (Figure S1a). We next investigated whether olfactory protection antibody- or T cell-mediated. Infection with the serologically distinct VSV-NJ strain establishes cell-mediated immune memory without nAb cross reactivity to VSV-IND (Lefrancois, 1984; Rosenthal and Zinkernagel, 1980). When VSV-NJ immune mice were challenged IN with VSV-IND, neither the OM nor the OB were protected (Figure 1d, e), suggesting antiviral T cells were insufficient for protection. These data established nAbs as critical to prevent viral OM infection and subsequent CNS neuroinvasion.

Because IP infection engendered protection without viral replication in the nose (Figure 1b,c), we tested whether systemic circulating antibodies provided adequate OM protection using passive antibody transfers. Naïve mice were challenged IN with VSV 12h after transfer of either VSV hyper-immune convalescent plasma or a monoclonal nAb against VSV (VI10) (Bachmann et al., 1997; Kalinke et al., 1996) (Figure 1f). OM viral titers in recipient mice were indistinguishable from those in naïve mice (Figure 1g). Accordingly, antibody transfer failed to prevent VSV neuroinvasion, and virus was readily detectable in the brain (Figure 1h) despite serum nAb titers similar to those in previously infected mice (Figure 1i).

To ensure that nAb titers achieved through passive transfer were sufficiently protective, we challenged mice subcutaneously (SC) (Moseman et al., 2012). When mice were challenged SC, both convalescent plasma and monoclonal antibody transfers prevented VSV replication in the draining lymph node (LN) (Figure 1j, Figure S1c). Since antibody could conceivably require >12hrs to protect the OM, we performed parabiosis between IP-infected and naïve mice to generate shared circulation and make their serum antibodies communal (Figure 1k). We challenged both parabionts IN two weeks following surgery and found that only the previously infected mice were protected from OM and OB infection (Figure 1l–m). This difference was observed despite equivalent serum nAb titers between partners (Figure 1n). Thus, the olfactory mucosa, analogous to the brain and retina (Iwasaki, 2017; Zhou and Caspi, 2010), was situated outside the protective reach of circulating antibody.

Systemic antibodies protect respiratory but not olfactory tissue in the URT

To address whether circulating antibody failed to protect the entire URT or merely the olfactory regions, we used Influenza/B/Malaysia/2506/2004 (Mal/04) which, unlike VSV, readily infects both OSNs and respiratory epithelial cells (Dumm et al., 2020). Similar to VSV, previous Mal/04 infection reduced viral OM titers upon rechallenge but convalescent plasma transfer did not prevent OM infection, despite similar nAb titers (Figure 2a–b). To directly compare antibody-mediated protection in respiratory and olfactory epithelia, we infected mT/mG mice IN with a Mal/04-Cre virus (Dumm et al., 2019), causing productively infected cells to lose constitutive membrane tdTomato and become membrane GFP+ (Muzumdar et al., 2007). Mal/04 infected both respiratory and olfactory cells in naïve mT/mG mice, but those receiving anti-Mal/04 convalescent plasma 12h before challenge had markedly decreased numbers of infected RE cells, while infection in the OE was unaffected (Figure 2c, d). These data suggested that within the nasal passages, blood-borne antibodies could protect the respiratory epithelium, but not olfactory epithelium.

Antibody fails to reach the olfactory mucosal surface

Our results indicated circulating antibodies readily protected the respiratory mucosa and LN but failed to protect the OM. To establish if systemic antibody could access olfactory tissue, we injected mice with an α-EpCAM antibody that binds both URT epithelial tissues. To unequivocally distinguish OE and RE, we used olfactory marker protein-GFP reporter mice (OMP-GFP) that fluorescently label OSNs. *Ex vivo* staining of OMP-GFP heads indicated α-EpCAM antibodies robustly label EpCAM in both olfactory and respiratory epithelium (Figure 3a). However, when antibody was injected IP 12h prior to sacrifice, only respiratory

epithelial cells were labeled! No staining of OM cells was observed (Figure 3b–c). Failure of specific antibody to exit circulation and bind olfactory targets indicated the presence of a vascular barrier that partitions olfactory tissue from circulation. Moreover, IN-administered α-EpCAM antibody prior to sacrifice led to staining of all EpCAM+ cells within the OM (Figure S2a–c), suggesting antibody moved freely within the OM and the impediment to antibody access lied at the vascular endothelium. This barrier remained intact both short- and long-term following IP VSV infection (Figures S2d–e). These data, in combination with our viral titer data, demonstrated that the blood-olfactory barrier (BOB) precluded systemic antibody from accessing olfactory tissue.

Extravascular plasma cells reside in the olfactory mucosa

Though serum antibody did not prevent olfactory infection, the humoral response nevertheless did (Figure 1b–e). How can this occur if blood antibody is unable to access the OM? Dimeric IgA protects other mucosal surfaces including the gut and lung (Mantis et al., 2011; Pilette et al., 2001); to determine whether URT protection was dependent on IgA antibodies, we IN VSV infected IgA-deficient ($IgA^{-/-}$) or $IgA^{+/-}$ mice. Upon rechallenge, $IgA^{-/-}$ mice were completely protected from OM infection (Figure 4a), indicating OM surface protection was not dependent on IgA.

Alternatively, we hypothesized antibody-secreting cells were recruited to olfactory tissue. If antibody-secreting plasma cells resided within the tissue, their local antibody production would bypass the BOB and provide antibodies directly to the mucosal surface. Indeed, using flow cytometry with IN antibody labeling to distinguish OM cells from contaminating nasal turbinate bone marrow (BM) cells (Figure S3a–e), OM plasma cell numbers were increased weeks after VSV infection (Figure 4b). While most OM plasma cells were intracellular IgA^+, IgG^+ or IgM^+ plasma cells were also detected (Figure 4c). Histologically, we identified $CD138^+$ plasma cells in the OM lamina propria of previously infected mice (Figure 4d).

Because antibody-secreting cells are typically quite rare, we quantified OM antigen-specific plasma cells using ELISpot assays. As expected, infected mice had increased α-VSV antibody-secreting cells in the BM compared to naïve controls (Figure S3f). To quantify α-VSV antibody-secreting cells in olfactory tissue, we dissected OM septum “peels” to avoid nasal turbinate BM cell contamination (Oberland and Neuhaus, 2014). IP infected mice had significantly increased numbers of α-VSV antibody-secreting cells within the OM (Figure 4e–f).

Human OM is anatomically similar to murine OM, but it is unknown if B cells reside in human olfactory tissue (Chen et al., 2014b; Mellert et al., 1991). We reanalyzed existing OM scRNA-seq data (Durante et al., 2020) from four healthy patient biopsies. Subsetting cells based on *Ig* gene expression, dimensionality reduction analysis and nearest-neighbor clustering unveiled two groups of B lineage cells (Figure 4g) containing cells from all four patients (Figure 4h). The differentially expressed genes between these clusters (Figure 4i) identified a small group as naïve B cells but also a large group of class-switched plasma cells (*JCHAIN, CD38, PRDM1*) within human OM. This group was $CD19^{lo}$HLA-

$DR^{lo}Ki\text{-}67^{-}CD95^{lo}$ $CD28^{+}$ compared to naïve B cells, indicating long-lived plasma cells (Mei et al., 2015).

Protection of the olfactory mucosa is dependent on local plasma cells

To determine if local plasma cells were responsible for OM protection, we systemically depleted plasma cells using bortezomib, a small-molecule proteasome inhibitor used clinically to treat multiple myeloma (Field-Smith et al., 2006). Bortezomib injection rapidly and specifically ablates plasma cells (Manning et al., 2015; Neubert et al., 2008), yet the long half-life of circulating antibody maintains systemic nAb titers following acute plasma cell depletion. Three weeks after VSV IP infection, plasma cells were depleted with bortezomib, and two weeks later, bortezomib-treated mice were rechallenged with VSV. Plasma cell-depleted mice remained protected from SC but not IN infection despite the presence of serum nAbs (Figure 5a–b, Figure S4a). ELISpots of OM tissue confirmed a reduction in olfactory plasma cells after bortezomib treatment (Figure S4b). We obtained similar results using marizomib, another selective plasma cell depletion molecule (Figure S4c–d). In both instances, plasma cell depletion allowed virus to reach the OB (Figure S4e–f).

As an alternative plasma cell depletion strategy, we used diphtheria toxin (DT)-mediated depletion of cells that have expressed activation-induced cytosine deaminase (AID). B cell activation and plasma cell differentiation is often accompanied by AID-dependent class switching and/or somatic hypermutation (Muramatsu et al., 2000). To selectively ablate B cells that had expressed AID, we IP infected $AID^{Cre/+}$ x inducible DTR (AID-DTR) mice, waited 21 days, and administered DT. Systemic depletion of class-switched B lineage cells abolished OM protection despite ample serum nAb titers (Figure 5c–d) and similarly enabled CNS neuroinvasion (Figure S4g). These data suggested plasma cells recruited to the OM protect the olfactory mucosal surface.

Lymph node CXCR3 signaling and T cell help spur plasma cells OM protection

Next, we attempted to discern the signals that drove plasma cells to the OM. Long-lived plasma cells typically reside in the BM to secrete antibody into circulation (Brynjolfsson et al., 2018; Lemke et al., 2016; Lightman et al., 2019). The chemokine receptor CXCR4 is critical to recruit and retain BM plasma cells (Cheng et al., 2018; Muehlinghaus et al., 2005; Nie et al., 2004). Alternatively, activated plasmablasts use the chemokine receptor CXCR3 to migrate into effector tissues (Chihara et al., 2013; Hauser et al., 2002; Marques et al., 2011). To determine if CXCR3 was required for OM plasma cell recruitment, we IP VSV infected *Cxcr3*$^{-/-}$ mice. *Cxcr3*-deficient mice generated serum nAbs but failed to completely protect the OM from IN reinfection (Figure 6a, b), which corresponded to a reduced number of OM VSV-specific plasma cells (Figure S5a). To temporally impair CXCR3 during the immune response, we administered an α-CXCR3 antibody or isotype control at days 3, 5, 7, and 10 following VSV infection. CXCR3 blockade had little impact on serum nAb titers; however, IN rechallenge led to OM viral replication (Figure 6c, d). Both CXCR3 deficiency and blockade similarly compromised OB protection (Figure S5b, c).

CXCR3 ligands are canonically produced in inflamed tissues, but qRT-PCR for CXCR3 ligands *Cxcl9* and *Cxcl10* (Groom and Luster, 2011; Müller et al., 2010; Van Raemdonck et al., 2015) in the OM 4.5 dpi revealed mRNA expression comparable to naïve mice (Figure 6e, f). Given that IP infected mice had no OM viral replication, we reasoned CXCR3-mediated lymphocyte interactions in the draining LNs may program plasma cell OM residency. Literature suggests CXCR3 acts within secondary lymphoid organs to influence B and T cell effector fates (Bowyer et al., 2018; Duckworth et al., 2021; Groom et al., 2012; Serre et al., 2012). Indeed, we found that *Cxcl9* and *Cxcl10* mRNA were upregulated in the peritoneal-draining mediastinal LNs 4.5d after IP infection (Figure 6g, h).

These data suggested CXCR3-mediated interactions in the LN, not in the OM, influenced B cell homing ability. The lymph node cytokine milieu during infection is impacted by many cell types, but we found depleting CD8+ T cells and NK cells did not affect OM protection (Figure S5d, e). However, CD4+ T cell depletion abolished OM protection (Figure 6i). Administration of α-CD40L antibody 3 dpi to disrupt contact-dependent T/B interactions prevented OM and OB protection from rechallenge (Figure 6i, Figure S5f), indicating that direct CD4+ help to B lymphocytes was required. Notably, high plasma nAb titers were still detectable (Figure 6j), implying CD4+ T cells provide signals to B cells that instruct OM homing and not just facilitate antibody production.

CXCR3 is expressed by both effector T and B lymphocytes (Groom and Luster, 2011). To interrogate which compartment required CXCR3 for OM humoral protection, we generated T cell *Cxcr3*-deficient (*Cxcr3*$^{-/-}$:*Tcra*$^{-/-}$ BM→ *Cxcr3*$^{-/-}$) and B cell *Cxcr3*-deficient (*Cxcr3*$^{-/-}$:*μMT* BM→ *Cxcr3*$^{-/-}$) mixed bone marrow chimeras (BMCs). Unlike WT BMC controls, neither T cell *Cxcr3*-deficient nor B cell *Cxcr3*-deficient mice showed OM protection (Figure 6k). The brains of these mice were similarly exposed to viral invasion (Figure S5g). Mixed BMCs produced blood-borne nAbs (Figure S5h), indicating CXCR3 on both B and T lymphocytes was required for proper mucosal plasma cell OM protection.

Because T cell help drives OM surface protection, we tested the importance of antibody class-switching. After IP VSV infection, class-switch deficient AID$^{-/-}$ mice generated normal plasma nAb titers, yet the OM and the OB were not protected upon IN challenge (Figure 6l, m, Figure S5i).

To rule out that an antibody class-switching defect could explain the lack of OM protection when CXCR3 was compromised, we treated plasma nAbs with 2-mercaptoethanol (2-ME) to disrupt polymeric IgM antibodies (Charan and Zinkernagel, 1986; Scott and Gershon, 1970). As expected, 2-ME treatment of AID$^{-/-}$ plasma eliminated VSV neutralizing capacity (Figure 6m). However, 2-ME treated plasma antibodies from *Cxcr3*$^{-/-}$ (Figure 6n) or α-CXCR3 treated (Figure 6o) mice remained highly neutralizing. CD4 depletion prior to infection abolished antibody class switch, but class switching remained intact in mice when α-CD40L blockade began d3 post infection (Figure 6p), indicating T cell help in humoral OM protection extended beyond B cell class-switching.

Two-dose mucosal adjuvant vaccinations protect the olfactory mucosa

OM antibody protection could prevent URT infection and transmission while also shielding the CNS. Stimulating protective OM humoral immunity is therefore critical for vaccine design. Our data suggested a protective vaccination approach should elicit strong neutralizing antibody but must also recruit plasma cells to the tissue. To establish if protein antigen was sufficient for OM protection, we IP immunized with UV-inactivated VSV (VSV-UV) (Bachmann et al., 1993). IP VSV-UV injection generated serum nAb titers that protected against SC viral challenge but did not protect the OM from IN rechallenge, suggesting protein antigen alone did not install protective OM immunity (Figures 7a–c). To enhance vaccine efficacy, we co-administered VSV-UV with traditional adjuvants alum or CpG. Compared to VSV-UV alone, both adjuvants provoked enhanced serum nAb titers and protected against SC VSV challenge (Figure 7a–b). However, none of these vaccine formulations were sufficient to protect the OM from IN VSV challenge (Figure 7c). These immunizations also failed to protect the brain from viral neuroinvasion (Figure S6a).

Mucosal vaccination approaches highlight immunization route and mucosal adjuvants to drive protection of barrier tissues (Lavelle and Ward, 2021; Oh et al., 2021; Renegar and Small, 1994; Sheikh-Mohamed et al., 2021). We thus immunized mice with VSV-UV and dmLT, a double mutant derivative of *E. coli* heat labile toxin modified for increased clinical safety. This adjuvant drives systemic and mucosal antibody responses when given mucosally or parenterally (Akhtar et al., 2021; Clements and Norton, 2018). dmLT delivered IP, IM, or IN raised the blood nAb titers compared to VSV-UV alone (Figure S6b), yet OM protection was rarely observed (Figure 7d). We then administered two dmLT doses via the same routes and observed IP dmLT boost prevented VSV OM infection (Figure 7e). Two-dose IP dmLT vacccination also protected the OB from viral neuroinvasion (Figure 7f). Critically, multiple doses of alum + VSV-UV failed to protect the OM (Figure 7e), indicating that boosting alone does not guarantee OM barrier protection, despite similar nAb titers and class switching between alum and dmLT boosted mice (Figure 7g, S6c). IN dmLT-adjuvanted immunization induced modest nAb titers and failed to protect the OM (Figure 7g) likely due to poor antigen retention, as much of the inoculating bolus was lost to swallowing or expulsion.

How did dmLT drive humoral OM protection? The BOB remained intact after two doses of dmLT (Figure S6d), so we hypothesized induction of CXCR3 ligands influenced plasma cell homing and analyzed the mediastinal LNs for *Cxcl9* and *Cxcl10* production after dmLT or alum immunization. Twelve hours after the second dose, we found mRNA expression of both ligands was significantly increased in dmLT-immunized mice (Figure 7h–i).

Numerous reports of COVID-19-induced anosmia are consistent with direct SARS-CoV-2 OM infection (Brann et al., 2020; Meng et al., 2020). The failure of multiple vaccination strategies to protect the OM led us to investigate whether clinically approved mRNA vaccines against COVID-19 are OM protective. We challenged Keratin18-hACE2 transgenic (K18) mice, a model widely used for SARS-CoV-2 (Fumagalli et al., 2021; Zheng et al., 2020), with a VSV-SARS-CoV-2 chimeric virus that expresses the SARS-CoV-2 spike protein in place of the VSV-G surface protein, leading to OM sustentacular cell infection (Case et al., 2020; Dieterle et al., 2020). Prior infection protected the OM from rechallenge,

while convalescent plasma did not (Figure 7j). We found that a single IM dose of the Pfizer-BioNTech mRNA vaccine (BNT162b2) significantly reduced OM viral titers 3d after IN challenge (Figure 7k), indicating that mRNA immunization strategies could drive a tissue-specific protective effect.

Discussion

Systemic antiviral antibody is widely assumed to correlate with sterilizing immunity in peripheral tissues. Recent animal studies of SARS-CoV-2 (Bergwerk et al., 2021; Bricker et al., 2020; Case et al., 2020; Corbett et al., 2021; Fröberg et al., 2021; Hassan et al., 2020; Horiuchi et al., 2021; McMahan et al., 2021; Zhou et al., 2021), as well as the frequency of SARS-CoV-2 infections in vaccinated individuals, have cast doubt on this assumption. The efficacy of circulating antibodies and vaccination in URT protection has received substantial debate and attention in recent years (Kato et al., 2013; Renegar et al., 2004; Subbarao et al., 2004). Our study provides a compelling solution to this dilemma; RE in the upper airway was protected by circulating antibody, but the OE was not. Our data described the mechanistic underpinning for this failure: the blood-olfactory barrier (BOB) at least partially compartmentalized the OM from circulation. The BOB thus required plasma cells to physically relocate beyond the endothelium to produce locally protective antibody.

Our data highlighted how URT heterogeneity (distinct respiratory and olfactory components) profoundly shaped the immune parameters required for surface protection. Further complicating the issue, olfactory-respiratory delineation is not always clear in humans, as the two tissues can become progressively metaplastic and intermingled due to age and prior infection (Mori et al., 2021; Paik et al., 1992). Previous work attempted to quantify URT antibody responses using saliva or nasal washes (Mades et al., 2021; Wagner et al., 1987). Washes are ill-suited to sample olfactory regions deep within the nasal cavity and may insufficiently capture the divergent OE and RE humoral responses.

The BOB to some extent impeded circulating molecules from entering the OM. With respect to large molecular weight molecules like immunoglobulins, the BOB operated similarly to the blood-brain barrier (BBB). Other studies suggest olfactory ensheathing cells surrounding olfactory nerve fascicles may segregate the olfactory nerve from blood (Beiersdorfer et al., 2020; Mori, 2018), but our data indicated antibodies cannot efficiently cross the olfactory endothelial barrier. Careful examination of the BOB's functional variations and characteristics remains necessary, especially in humans, as these will impact drug delivery, including therapeutic antibodies for olfactory disorders. Nonetheless, our data demonstrated that OE junctions were not restrictive to antibody movement, as locally produced and IN-administered antibody could diffuse throughout the OM. Clinically, so-called "nose-to-brain" drug delivery relies on diffusion through the olfactory tract (Kumar et al., 2018; Lochhead and Thorne, 2012; Martin et al., 2021). The BOB may prevent systemic molecules from traveling up the olfactory tract into the brain, acting as an extension of the BBB.

The dichotomy between URT olfactory and respiratory epithelia is conserved across terrestrial mammal species (Green et al., 2012), hence our data may impact animal and human disease. Viruses, bacteria, and eukaryotic pathogens are all capable of accessing

the CNS through the human olfactory portal (Aronsson et al., 2003; Dando et al., 2014; Lawler and Stevenson, 2017; Moseman, 2020; Shivkumar et al., 2013). OM protection against potentially lethal diseases would require immunization strategies that recruit local plasma cells to secrete protective antibody. While we envision the greatest functional impact from olfactory plasma cells that secrete nAbs, many antibodies rely on Fc effector functions or combinatorial binding. Evidence suggests Fc-mediated functions influence olfactory immunity (Glauser et al., 2019), perhaps by acting through OM parenchymal cells or macrophages (Mellert et al., 1991). At a population level, humoral olfactory protection limits dissemination of respiratory pathogens. Pathogens replicate in the OM prior to encountering blood antibody pressure, and vaccinations that fail to induce olfactory protection may facilitate continued transmission and viral evolution. Recent studies have indicated nasal viral replication can occur in the presence of anti-SARS-CoV-2 antibody (Corbett et al., 2021; Fröberg et al., 2021; Horiuchi et al., 2021; McMahan et al., 2021), and puzzlingly, breakthrough infections are not associated with waning antibody titers (Terreri et al., 2022). One possible factor in mild breakthrough cases could be an olfactory foothold for viral replication prior to virus being squashed by the systemic immune response in other tissues. This hypothesis is corroborated by the observation that breakthrough infections typically present with mild pulmonary symptoms (Bergwerk et al., 2021). Olfactory infection is one of many elements that could impact breakthrough cases, including weak antibody affinity, viral mutations, and antibody transudation efficacy.

Tissue-resident T lymphocytes have been the subject of intense research over the past decade; more recently, several studies have described the existence and importance of tissue-resident memory B cells in humans and animals (Allie et al., 2019; Johnson et al., 2020; Niimi et al., 2018; Oh et al., 2021; Tan et al., 2022; van der Feltz et al., 2001; Weisel et al., 2022, 2020). While memory B and T cells in the OM could contribute to a secondary response (Iijima and Iwasaki, 2016; Oh et al., 2019), plasma cells that provide a continuous antibody “shield” at the mucosal surface would be critical to thwart neuroinvasion.

Our data demonstrated that OM plasma cells provided a non-redundant barrier against IN viral challenge. Polymeric Igs (especially dimeric IgA) are thought to protect mucosal surfaces by binding to the polymeric Ig-receptor (Chen et al., 2020; Horton and Vidarsson, 2013; Yu et al., 2018). We found IgA was dispensable for OM protection, and IgM was unable to protect. While protective meningeal IgA-secreting plasma cells were recently described (Fitzpatrick et al., 2020), and many olfactory plasma cells expressed IgA, plasma cell placement beyond the BOB is what determined olfactory protection. Blood IgA titers have been used as a surrogate for mucosal protection (Pakkanen et al., 2010), but it is likely that OM plasma cells are uncoupled from the serum IgA response (Mazanec et al., 1989). Whether other mucosal sites recruit similar plasma cell populations following infection requires additional work.

Our data indicated olfactory plasma cell recruitment depended on CXCR3 and correlated with LN *Cxcl9/10* expression. The cellular source of CXCL9/10 was unclear, although these chemokines are induced by IFNs (Sung et al., 2012) and T cell-derived IFN may spur LN *Cxcl9* and/or *Cxcl10* expression. Our mixed BMC data suggested B cell-intrinsic differences between nascent plasma cells fated for olfactory homing and typical BM-homing plasma

cells. Priming of B cells with predefined fates is a poorly understood issue, but recent work suggests “type 1” B cells may protect barrier tissues from viral infection (Keller et al., 2021; Naradikian et al., 2016; Serre et al., 2012; Song et al., 2022). IP infection triggers strong type 1 signals, robust T cell activation, and IFN production, stimuli which may affect this plasma cell localization phenotype. OM protection was severely compromised in CXCR3-deficient animals, but slightly better than naïve animals, indicating alternative plasma cell recruitment/differentiation pathways may be involved. Many questions remain regarding olfactory plasma cells. Are these cells stationed in a specific tissue niche? How long do they reside, and what molecules retain them? Do these cells proliferate *in situ* or recirculate to patrol other tissues? How are OM and BM plasma cells clonally related?

Our data showed that the pleiotropic effects of dmLT (Akhtar et al., 2021), but not alum, immunization generated sterilizing OM immunity, but other adjuvant and dosing combinations may suffice. The OM protection observed after single-dose Pfizer-BioNTech vaccination suggested mRNA vaccines may be suited toward producing this type of immunity. Intranasal vaccination has been proposed as an effective, convenient mechanism to elicit mucosal protection (Fehervari, 2021; Hassan et al., 2020; Oh et al., 2021), and this approach warrants further investigation, despite the low antibody titers induced in our mouse model. “Prime and pull” immunization (a mucosal booster dose) (Shin and Iwasaki, 2012) may potentially draw plasma cells into the OM. Our discovery of a BOB provides important insight for designing vaccines that protect the olfactory tract from both respiratory and neuroinvasive pathogens.

Limitations of the study

While our study demonstrated the existence of a blood-olfactory barrier and protective olfactory plasma cells in mice, it remains to be seen whether this physiology is recapitulated in humans or other animals. We identified use of the adjuvant dmLT as protective, but other vaccine adjuvants may suffice, and the effects of vacciniation may differ in humans. Our data showed that CXCR3 was required in both T and B cells for olfactory protection, and CXCR3 ligands were upregulated in the draining lymph node, we did not determine the cellular source of these ligands. Protection of the olfactory mucosa was dependent on neutralizing antibodies produced by mucosal plasma cells, but T cell-mediated immunity and non-neutralizing antibodies may still impact immunity in the nasal mucosa.

STAR METHODS

RESOURCE AVAILABILITY

Lead contact—Further information and requests for resources and reagents should be directed to and will be fulfilled by the lead contact, Ashley Moseman (ashley.moseman@duke.edu).

Materials availability—This study did not generate new unique reagents.

Data and code availability

- This paper analyzes existing, publicly available single-cell RNA sequencing data. These accession numbers for the datasets are listed in the Key Resources Table.
- All original code has been deposited on GitHub and is publicly available as of the date of publication. DOIs are listed in the Key Resources Table.
- Any additional information required to reanalyze the data reported in this paper is available from the lead contact upon request.

EXPERIMENTAL MODEL AND SUBJECT DETAILS

Mice—B6, mT/mG, Cxcr3$^{-/-}$, μMT Tcra$^{-/-}$, AID$^{Cre/+}$, AID$^{-/-}$, iDTR, K18 mice (see Key Resources Table) were purchased from the Jackson Laboratory and either used or bred in-house. OMP-GFP on C57BL/6 background (Potter et al., 2001) mice were provided by Dorian McGavern (NINDS). Mice were bred and maintained under specific pathogen-free conditions at Duke University School of Medicine. Mice used in this study were between 6 and 14 weeks of age. Male and female mice were equally represented across experiments (no phenotypic differences between male and female mice were observed). All mice in this study were handled in accordance with the guidelines set forth by the Duke Animal Care and Use Committee.

Viruses—Vesicular stomatitis virus ovalbumin, serotype Indiana (VSV-OVA, VSV, or VSV-IND) and VSV-OVA, serotype NJ (VSV-NJ) (provided by Dorian McGavern, NINDS) were propagated on Vero cells. VSV-Sars-S-GFP (gift of Sean Whelan, Washington University School of Medicine in St. Louis) was propagated on VeroE6 cells overexpressing human TMPRSS2 protease. Influenza B/Malaysia/2506/2004 (Mal/04) and Mal/04-Cre expressing viruses (provided by Nicholas Heaton, Duke) were grown in embryonated chicken eggs in a humidified incubator at 33°C and Mal/04 assays were performed on MDCK cells. See Key Resources Table for virus identifiers.

Cell lines—Vero cells were epithelial kidney cells orginially derived from adult African green monkey and maintained in MEM (10% FBS, 1% Pen/Strep, 1% NEAA, 1% Sodium Pyruvate). Vero-E6 cells overexpressing human TMPRSS2 were originally cloned from Vero 76 and maintained in the same Vero media. MDCK cells were orginally derived from adult female canine kidney tissue and grown in MEM (5% FBS, 1% Pen/Strep, 1% Glutamax, 2% Sodium Bicarbonate, 2% HEPES). See Key Resources Table for more information.

METHOD DETAILS

Viral Titer Quantification—Plaque/focus-forming assays were performed to quantify VSV and Mal/04 viral titers, while qRT-PCR was used to quantify VSV-Sars-S-GFP titer. Briefly, animals were perfused intracardially with PBS and tissues (olfactory mucosa, olfactory bulb, lung, popliteal lymph nodes) were snap frozen on dry ice. Tissues were immersed in 1 mL of 2% FBS MEM containing zirconia silica beads (Biospec Products #11079125z) and homogenized for 1 min using a Biospec Products Mini Beadbeater.

Plaque/focus-forming assays ––—For VSV, plaque assays were performed by spinning homogenates for 10 min at 1500 x g/4°C and serially diluting supernatants in MEM for quantification on Vero cells. One-hundred microliters of diluted homogenate were added to Vero monolayers in flat-bottom 24-well plates and incubated for ~1 hour at 37°C in 5% CO_2. Four hundred microliters of 1% methylcellulose in MEM were added to each well, and plates were incubated for 18-24 hrs. Cells were subsequently fixed with 1.25% neutral buffered formalin (10 min), stained with crystal violet (10 min), and plaques were enumerated. For Mal/04, focus-forming assays were performed by spinning homogenates for 10 min at 1500 x g/4°C and serially diluting supernatants in Infection PBS (35% BSA, 1% Pen-Strep, 1% Ca+ Mg+ in PBS) for quantification on MDCK cells. One-hundred microliters of diluted homogenate were added to MDCK monolayers in flat-bottom 24-well plates and incubated for ~1 hour at 37°C in 5% CO_2. Four hundred microliters of agar overlay (0.01% DEAE Dextran, 0.066% $NaHCO_3$, 0.5% Oxoid agar, 22% dH_2O, 0.1% Trypsin in MEM) were added to each well, and plates were incubated for 24-36 hrs. To enumerate influenza focus-forming units, Cells were subsequently fixed with 1.25% neutral buffered formalin (10 min), washed with PBS, treated with 300 μL primary antibody (1:1000 hyperimmune α-Mal/04 serum), and incubated for 1 hr at RT with gentle shaking. Cells were washed with PBS and 300 μL secondary antibody (1:2000 Peroxidase-conjugated AffiniPure Goat Anti-Mouse IgG 0.8/mL, Jackson Immunoresearch) was added, incubating on shaker at RT for 45 min before washing with PBS and adding 200 μL AEC substrate (SeraCare KPL TrueBlue Substrate) per well. After 10 min of RT incubation, plates were washed, and focus-forming units were quantified.

qRT-PCR ––—VSV-Sars-S-GFP was quantified via qRT-PCR. Virally infected tissues (olfactory mucosa) were harvested and snap frozen. Tissues were homogenized with zirconia/silica beads using a tissue beater in RNA lysis buffer (Qiagen). Homogenates were centrifuged for 10 min at 1500 x g/4°C. Viral RNA was extracted from clarified supernatant using QIAamp Viral RNA kit (see Key Resources Table). Quantitative PCR was performed using EXPRESS One-Step Superscript qRT-PCR kit (see Key Resources Table) and using 18S rRNA as an endogenous control (ThermoFisher Scientific, #4319413E) using the QuantStudio 6 pro instrument (ThermoFisher). Gene expression was plotted on an arbitrary standard curve then normalized to 18S in the same sample using QuantStudio Design and Analysis Software (ThermoFisher). Quantification of viral reads (in duplicates) was performed with the following custom primers and probes (IDT) (Sequences provided in the Key Resources Table) : SARS CoV-2 S FWD, SARS CoV-2 S REV, SARS CoV-2 S Probe, Eukaryotic 18s rRNA Endogenous Control

Neutralizing Antibody Titers VSV ––—Mice were bled retro-orbitally with heparinized tubes and whole blood was centrifuged at 2,000 x g for 10 minutes at 4°C. Plasma was taken, serially diluted two-fold in MEM, and mixed with VSV (50 PFU/well) in 96-well plates. After incubating for 90 minutes at 37°C, 100 μL of plasma/virus mixture was added to monolayers of Vero cells in a 96-well plate. Cells were incubated for 1 hr at 37°C and 5% CO_2 before adding 100 μL of 1% methylcellulose overlay. After 18-24 hrs of incubation, cells were fixed with 1.25% neutral buffered formalin, stained with crystal violet, and

plaques enumerated. The highest dilution that reduced plaque numbers by >50% was taken as the neutralizing antibody titer.

Influenza B Mal/04 ––—Serum was obtained as with VSV and serially diluted in Infection PBS (see "Viral Titer Quantification"). Diluted serum was incubated with Influenza B Mal/04 (50 PFU/well) for 90 minutes at 37°C. 100 μL of serum/virus mixture was added to monolayers of MDCK cells in a 96-well plate and incubated for 1 hr at 37°C and 5% CO_2. 100 μL of oxoid agar overlay (see "Viral Titer Quantification") was then added to each well, incubated 24-36 hours, and cells were fixed and stained as described in focus-forming assay. The highest dilution that reduced focus numbers by >50% was taken as the neutralizing antibody titer.

Infections—*VSV* Eight to fourteen-week-old mice were infected intranasally (IN) by pipetting 10 μL of viral diluent in each nostril (1 x 10^5 PFU total) under anesthesia. For intraperitoneal (IP) infections, mice were infected with 5 x 10^6 PFU of VSV. For subcutaneous challenge (SC) experiments, mice were infected via hock injection with 25 μL per hind leg (1 x 10^5 PFU total). *Influenza B Mal/04* Eight to twelve-week-old mice were infected IN by pipetting 25 μL of viral diluent in each nostril (5 x 10^5 PFU total) under isoflurane anesthesia.

VSV-Sars-S-GFP Eight to twelve-week-old mice were infected IN by pipetting 25 μL of viral diluent in each nostril (1.25 x 10^5 PFU total) under anesthesia.

Antibody transfers—Anti-VSV hybridoma producing the neutralizing monoclonal murine IgG2a antibody (VI10) was generated as previously described (Kalinke et al., 1996) and a kind gift from Matteo Iannacone (Ospedale San Raffaele, Milan, Italy). Convalescent plasma specific for VSV and Mal/04 Influenza B were generated by repeated infections with each respective virus to create hyperimmune mice. Mice were bled retro-orbitally with heparinized tubes following infectious boosts, and finally terminally bled by cardiac puncture before whole blood was centrifuged at 2,000 x g for 10 minutes at 4°C. In each experiment, mice received 500 μL of plasma IP 12 hours prior to infection.

Parabiosis—Surgeries were performed as previously described (Wright et al., 2001). Briefly, mice (1 VSV IP-infected d21 partner, 1 naïve partner) were anesthetized using a solution of 90 mg/kg Ketamine, 10 mg/kg Xylazine, and 2 mg/kg Acepromazine in PBS. Hair removal cream was applied to the sides of both mice and a sterile incision was made from the forelimb elbow to the hindlimb knee. Sutures were used to join the forelimbs and hindlimbs of the animals at the joints, and the skin flaps of both animals were sutured together. Surgical staples were used to reinforce the attachment before being removed 1 week after surgery.

Immunohistochemistry—Mice were perfused intracardially with 2.5% neutral buffered formalin (NBF) and skin around the head and nose was removed before fixing whole heads in 2.5% NBF overnight at 4°C. Heads were then submerged in a 0.5 M EDTA solution for 5-7 days at 4°C to decalcify bone around the olfactory regions. Once decalcified, heads were embedded in tissue freezing medium (Triangle Biomedical Sciences) for sagittal or coronal

sections. Cryosections were cut using a Leica CM1850 cryostat at a thickness of 30 μm after which sections were washed and stained in PBS. Primary antibodies were incubated on cryosections overnight at 4°C, and secondary staining was done for 2 hrs at 4°C. After staining, sections were washed 4-5 times with PBS, and 2-3 drops of Mowiol Mounting Media (9.6% (w/v) Mowiol 4-88, 24% (w/v) glycerol, 2.5% DABCO, 0.1 M Tris-Cl pH 8.5 in water) were added to each section before addition of a coverslip. Images were acquired using a Leica SP8 Upright Confocal Microscope equipped with 405 nm diode laser, Argon/2 (458, 488, 514 nm) laser, 561 nm diode laser, and HeNe 633 nm laser. Image analysis was performed using Imaris software (Bitplane) version 7.6.1.

Quantification of viral infection by immunohistochemistry—mT/mG mice were infected IN with Mal/04-Cre virus (5 x 10^6 FFU). Four mice were used as naïve controls, and four mice received IP injections of 500 μL of convalescent plasma per mouse 12 hours prior to infection. Three sagittal sections per mouse were prepared and stained with DAPI (1.25 μg/mL). Infected (mGFP+) cells were quantified per mm of olfactory epithelium or respiratory epithelium.

In vivo α-EpCAM antibody treatment—20 μg of α-EpCAM antibody (see Key Resources Table for antibodies) in 100 μL PBS were injected IP into OMP-GFP mice 12 hours prior to sacrifice. Sagittal sections were prepared as described in "Immunohistochemistry" above. For quantification of EpCAM staining, six serial sections from two mice were prepared. Half of the sections were stained *ex vivo* for positive controls of EpCAM biodistribution, with the same α-EpCAM antibody (5 μg/mL). These positive controls then received donkey α-rat-AlexaFluor647 (2.5 μg/mL) and DAPI (1.25 μg/mL) as a secondary stain. The other sections, having received only in vivo α-EpCAM antibody were stained ex vivo with only donkey α-rat-AlexaFluor647 (2.5 μg/mL) and DAPI (1.25 μg/mL). Tile scan images of the entire head were captured using the Leica SP8 Confocal Microscope. Image analysis was performed using Imaris software (Bitplane) version 7.6.1. To quantify EpCAM signal in olfactory and respiratory regions, custom surfaces were drawn using OMP-GFP signal as a demarcation between olfactory and respiratory epithelium. The intensity sum of the EpCAM signal with background subtraction was calculated for each surface. This value was normalized to the DAPI intensity sum to account for variation in region size, achieving a normalized EpCAM intensity value.

Flow Cytometry and Cell Isolation—Five minutes prior to sacrifice, 5 μL of α-CD45.2 antibody (see Key Resources Table for all antibodies and dilutions) was pipetted into both nostrils of each mouse (1 μg total). Mice were perfused intracardially with saline solution prior to harvesting organs and mincing with scissors. Tissues were digested in 0.5 mL Hibernate A with DNase I (Roche, 0.5 mg/mL) and Collagenase D (Roche, 0.5 mg/mL) at 37°C for 30 min with constant shaking. Cells were washed, spun down at 500 x g for 5 min, and resuspended in PBS. Cells were stained on ice for 20 min with α-B220, Zombie UV Viability dye, and α-CD45. Cells were then washed, spun down at 500 x g for 5 min, and fixed and permeabilized with True-Nuclear Fix/Perm Buffer system (Biolegend) as directed. Cells were then stained with α-IgG, α-IgA, and α-IgM in True Nuclear Perm Buffer (Biolegend) on ice for 20 min. Cells were washed with True Nuclear Perm Buffer and

analyzed on a BD Fortessa-X20 Flow Cytometer equipped with five lasers (UV, 405, 466, 561, and 640 nm excitation). Data analysis was conducted in FlowJo 10.8.1.

B cell Enzyme-linked Immunospot Assay (ELISpot)—PVDF 96-well plates (MabTech) were prewet with 15μL of 35% ethanol and incubated for 30 seconds. The ethanol was then firmly shaken-out and wells were immediately rinsed 2x with 200 μL of PBS. 50 μL of VSV-containing supernatant (10^8 PFU equivalent) was added as antigen to each well before incubation overnight at 4°C. Antigen solution was then removed from the wells and washed 3x with 200 μL PBS. The plate was incubated for 1 hr at RT with 200 μL of blocking buffer (RPMI, 5% FBS, 0.01% PenStrep, and 0.01% GlutaMAX). Cells were harvested from mouse bone marrow or olfactory mucosa septum peel (OM). The plate was decanted and cells were seeded onto plates at two separate dilutions with 3 replicates per dilution in RPMI blocking buffer, 100 μL/well. BM cells were seeded at 2 x 10^6 or 5 x 10^5 cells/well, and OM peels were seeded in two dilutions dependent on the total number of cells available. Plates were incubated overnight at 37°C and 5% CO_2 before removing the cells and rinsing twice in 200 μL PBS. The empty plate was rinsed 5 times in wash buffer (0.025% Tween-20 in PBS) before incubation at RT for 2 hours with 100 μL of diluted biotinylated detection antibody (Peroxidase-conjugated AffiniPure Goat Anti-Mouse IgG 0.8/mL, Jackson Immunoresearch) diluted 1:2500 in PBS. The plate was then emptied and the underdrain removed prior to washing both sides of the plate 5 times with Tween-20 wash buffer. The plates were subsequently incubated for 30 minutes at RT in the dark with AEC substrate (100 μL/well, SeraCare KPL TrueBlue Substrate). Color development was stopped by rinsing both sides of the plate with DI water and air dried in the dark. Once dry, spots were enumerated and the average of all 6 replicates for each sample was calculated.

In vivo depletion/blockade studies—CXCR3 blockade was performed by IP administration of α-CXCR3 antibody (see Key Resources Table for all depleting/blocking antibodies) at days 3 (250 μg/mouse), 5 (500 μg), 7 (500 μg), and 10 (250 μg) post-infection. For CD4+ T cell depletion, α-CD4 antibody was injected IP 1 day prior to infection (500 μg/mouse). CD40L blockade was done by IP dose of α-CD40L antibody at day 3 following infection (250 μg/mouse). CD8+ T cell depletion was performed by giving α-CD8 antibody IP 1 day prior to infection (250 μg) and 4 days after infection (100 μg). For NK cell depletion, α-NK1.1 antibody was injected IP 1 day prior to infection (250 μg) and 4 days after infection (100 μg). For plasma cell depletions, mice were infected with VSV-IND at least three weeks prior to plasma cell depletion. Mice were treated with 3 μg of Bortezomib (5 mg/mL in DMSO, diluted in PBS to 100 μL/mouse) or 1 μg of Marizomib (0.2 mg/mL in DMSO, diluted in PBS to 100 μL/mouse) on days 22- and 26-post infection and rested until prior to rechallenge (d40). For AID-Cre DTR experiments mice were administered 1 μg diphtheria toxin (DT) IP three weeks following infection, followed by 14 days of rest prior to rechallenge.

Cxcl9/10 qRT-PCR—B6 Mice were infected IP with VSV and tissues (olfactory mucosa, medisastinal lymph nodes) were harvested and snap frozen. qRT-PCR was performed as described above. Quantification of viral reads (in duplicates) was performed with the following custom primers and probes (IDT) (Sequences provided in the Key Resources

Table): *Cxcl9* FWD, *Cxcl9* REV, *Cxcl9* Probe, *Cxcl10* FWD, *Cxcl10* REV, *Cxcl10* Probe, Eukaryotic 18s rRNA Endogenous Control, Assay ID: Hs99999901_s1; ABY-QSY Jira 56112

Mixed Bone Marrow Chimeras—Eight-week-old *Cxcr3*$^{-/-}$ mice were irradiated with 840 rads using a Precision X-RAD 225Cx. Four hours following X-ray irradiation, mice were reconstituted with the following combinations of bone marrow: WT, *Cxcr3*$^{-/-}$:μMT (30:70), *or Cxcr3*$^{-/-}$+*Tcra*$^{-/-}$ (30:70) (~2 x 10^6 cells/mouse, IV injection). Eight weeks following bone marrow transfer mice were infected and rechallenged as indicated in "Infections".

Vaccinations—VSV was propagated in Vero cells prior to concentration and inactivation for vaccine adjuvant. Vero media was harvested, centrifuged at 2,000 x g for 5 minutes, and the supernatant containing virus was passed through a 0.22 micron filter. Virus was concentrated by ultracentrifugation for 90 minutes at 40,000 x g and 4°C. VSV was then inactivated by exposing to UV light (1 cm from 30 W UV bulb) for 3 hours. Complete VSV inactivation was confirmed by plaque-forming assay. VSV-UV (50 μL/mouse) was mixed with various adjuvants (see Key Resources Table): Imject alum (50 μL/mouse), CpG (2 μg/mouse in 50 μL PBS), dmLT (5 μg/mouse in 50 μL PBS). Total volume for all IP and intramuscular immunizations was 100 μL, and immunization dose was halved for IN immunizations. Pfizer-BioNTech vaccine was administered IM (50 μL, 5 μg) to mice 21d prior to IN challenge.

Bioinformatic analysis—All analysis of single-cell RNAseq data was conducted in R v4.0.3 and Seurat v4.1.0. Data was obtained from Durante et. al. 2020 (Durante et al., 2020) (see Key Resources Table). Briefly, UMAP dimensional reduction and nearest neighbor clustering was used to identify immune cell clusters with high *Ptprc* gene expression. Further subsetting, UMAP dimensional reduction, and clustering was used to identify B cell subsets based on *Ig* gene expression. Differentially expressed genes were used to identify and name these groups. All code is deposited on GitHub (see Key Resources Table).

QUANTIFICATION AND STATISTICAL ANALYSIS

Statistical analysis and graphics—All statistical analyses were performed in GraphPad Prism 9.1.2 as indicated in the figure legends. Plots were generated in Prism and original diagrams were created with BioRender.com.

Supplementary Material

Refer to Web version on PubMed Central for supplementary material.

Acknowledgments

EAM is partially supported by 1R01NS121067, 1R21AG074324, and by the Duke School of Medicine Whitehead Family Scholarship. SAW received support from T32AI052077. We would like to acknowledge Garnett Kelose, Maria Ciofani, and Ed Miao for contributing mice and the Kelsoe lab for helpful discussions.

References

Akhtar M, Nizam NN, Basher SR, Hossain L, Akter S, Bhuiyan TR, Qadri F, Lundgren A, 2021. dmLT Adjuvant Enhances Cytokine Responses to T Cell Stimuli, Whole Cell Vaccine Antigens and Lipopolysaccharide in Both Adults and Infants. Front. Immunol 12.

Allie SR, Bradley JE, Mudunuru U, Schultz MD, Graf BA, Lund FE, Randall TD, 2019. The establishment of resident memory B cells in the lung requires local antigen encounter. Nat. Immunol 20, 97–108. 10.1038/s41590-018-0260-6 [PubMed: 30510223]

Aronsson F, Robertson B, Ljunggren H-G, Kristensson K, 2003. Invasion and persistence of the neuroadapted influenza virus A/WSN/33 in the mouse olfactory system. Viral Immunol. 16, 415–423. 10.1089/088282403322396208 [PubMed: 14583155]

Bachmann MF, Kalinke U, Althage A, Freer G, Burkhart C, Roost HP, Aguet M, Hengartner H, Zinkernagel RM, 1997. The role of antibody concentration and avidity in antiviral protection. Science 276, 2024–2027. 10.1126/science.276.5321.2024 [PubMed: 9197261]

Bachmann MF, Kündig TM, Kalberer CP, Hengartner H, Zinkernagel RM, 1993. Formalin inactivation of vesicular stomatitis virus impairs T-cell- but not T-help-independent B-cell responses. J. Virol 67, 3917–3922. [PubMed: 8389912]

Baden LR, El Sahly HM, Essink B, Kotloff K, Frey S, Novak R, Diemert D, Spector SA, Rouphael N, Creech CB, McGettigan J, Khetan S, Segall N, Solis J, 2021. Efficacy and Safety of the mRNA-1273 SARS-CoV-2 Vaccine | NEJM [WWW Document]. URL 10.1056/nejmoa2035389 (accessed 3.22.22).

Barrios AW, NÃ°Ã±ez G, SÃinchez Quinteiro P, Salazar I, 2014. Anatomy, histochemistry, and immunohistochemistry of the olfactory subsystems in mice. Front. Neuroanat 8, 1–10. 10.3389/fnana.2014.00063 [PubMed: 24523676]

Bauer L, Laksono BM, de Vrij FMS, Kushner SA, Harschnitz O, van Riel D, 2022. The neuroinvasiveness, neurotropism, and neurovirulence of SARS-CoV-2. Trends Neurosci. S0166-2236(22)00050–9. 10.1016/j.tins.2022.02.006

Beiersdorfer A, Wolburg H, Grawe J, Scheller A, Kirchhoff F, Lohr C, 2020. Sublamina-specific organization of the blood brain barrier in the mouse olfactory nerve layer. Glia 68, 631–645. 10.1002/glia.23744 [PubMed: 31696993]

Bergwerk M, Gonen T, Lustig Y, Amit S, Lipsitch M, Cohen C, Mandelboim M, Levin EG, Rubin C, Indenbaum V, Tal I, Zavitan M, Zuckerman N, Bar-Chaim A, Kreiss Y, Regev-Yochay G, 2021. Covid-19 Breakthrough Infections in Vaccinated Health Care Workers | NEJM [WWW Document]. URL 10.1056/NEJMoa2109072 (accessed 3.22.22).

Bosch AATM, Biesbroek G, Trzcinski K, Sanders EAM, Bogaert D, 2013. Viral and Bacterial Interactions in the Upper Respiratory Tract. PLOS Pathog. 9, e1003057. 10.1371/journal.ppat.1003057 [PubMed: 23326226]

Bowyer G, Grobbelaar A, Rampling T, Venkatraman N, Morelle D, Ballou RW, Hill AVS, Ewer KJ, 2018. CXCR3+ T Follicular Helper Cells Induced by Co-Administration of RTS,S/AS01B and Viral-Vectored Vaccines Are Associated With Reduced Immunogenicity and Efficacy Against Malaria. Front. Immunol 9, 1660. 10.3389/fimmu.2018.01660 [PubMed: 30090099]

Brann DH, Tsukahara T, Weinreb C, Lipovsek M, Van den Berge K, Gong B, Chance R, Macaulay IC, Chou HJ, Fletcher RB, Das D, Street K, de Bezieux HR, Choi YG, Risso D, Dudoit S, Purdom E, Mill J, Hachem RA, Matsunami H, Logan DW, Goldstein BJ, Grubb MS, Ngai J, Datta SR, 2020. Non-neuronal expression of SARS-CoV-2 entry genes in the olfactory system suggests mechanisms underlying COVID-19-associated anosmia. Sci. Adv 6, 5801–5832. 10.1126/sciadv.abc5801

Bricker TL, Darling TL, Hassan AO, Harastani HH, Soung A, Jiang X, Dai Y-N, Zhao H, Adams LJ, Holtzman MJ, Brett Case J, Fremont DH, Klein R, Diamond MS, M Boon AC, 2020. A single intranasal or intramuscular immunization with chimpanzee adenovirus vectored SARS-CoV-2 vaccine protects against pneumonia in hamsters. bioRxiv 2020.12.02.408823-2020.12.02.408823. 10.1101/2020.12.02.408823

Brynjolfsson SF, Persson Berg L, Olsen Ekerhult T, Rimkute I, Wick M-J, Mårtensson I-L, Grimsholm O, 2018. Long-Lived Plasma Cells in Mice and Men. Front. Immunol 9.

Busse WW, 1991. Pathogenesis and Sequelae of Respiratory Infections. Rev. Infect. Dis 13, S477–S485. [PubMed: 1862278]

Butowt R, Meunier N, Bryche B, von Bartheld CS, 2021. The olfactory nerve is not a likely route to brain infection in COVID-19: a critical review of data from humans and animal models. Acta Neuropathol. (Berl.) 141, 809–822. 10.1007/s00401-021-02314-2 [PubMed: 33903954]

Case JB, Rothlauf PW, Chen RE, Kafai NM, Fox JM, Smith BK, Shrihari S, McCune BT, Harvey IB, Keeler SP, Bloyet LM, Zhao H, Ma M, Adams LJ, Winkler ES, Holtzman MJ, Fremont DH, Whelan SPJ, Diamond MS, 2020. Replication-Competent Vesicular Stomatitis Virus Vaccine Vector Protects against SARS-CoV-2-Mediated Pathogenesis in Mice. Cell Host Microbe 28, 465–474.e4. 10.1016/j.chom.2020.07.018 [PubMed: 32798445]

Ceban F, Ling S, Lui LMW, Lee Y, Gill H, Teopiz KM, Rodrigues NB, Subramaniapillai M, Di Vincenzo JD, Cao B, Lin K, Mansur RB, Ho RC, Rosenblat JD, Miskowiak KW, Vinberg M, Maletic V, McIntyre RS, 2022. Fatigue and cognitive impairment in Post-COVID-19 Syndrome: A systematic review and meta-analysis. Brain. Behav. Immun 101, 93–135. 10.1016/j.bbi.2021.12.020 [PubMed: 34973396]

Charan S, Zinkernagel RM, 1986. Antibody mediated suppression of secondary IgM response in nude mice against vesicular stomatitis virus. J. Immunol 136.

Chen CR, Kachramanoglou C, Li D, Andrews P, Choi D, 2014a. Anatomy and cellular constituents of the human olfactory mucosa: a review. J. Neurol. Surg. Part B Skull Base 75, 293–300. 10.1055/s-0033-1361837

Chen CR, Kachramanoglou C, Li D, Andrews P, Choi D, 2014b. Anatomy and cellular constituents of the human olfactory mucosa: a review. J. Neurol. Surg. Part B Skull Base 75, 293–300. 10.1055/s-0033-1361837

Chen K, Magri G, Grasset EK, Cerutti A, 2020. Rethinking mucosal antibody responses: IgM, IgG and IgD join IgA. Nat. Rev. Immunol 20, 427–441. 10.1038/s41577-019-0261-l [PubMed: 32015473]

Cheng Q, Khodadadi L, Taddeo A, Klotsche J, F Hoyer B, Radbruch A, Hiepe F, 2018. CXCR4-CXCL12 interaction is important for plasma cell homing and survival in NZB/W mice. Eur. J. Immunol 48, 1020–1029. 10.1002/eji.201747023 [PubMed: 29427452]

Chihara N, Aranami T, Oki S, Matsuoka T, Nakamura M, Kishida H, Yokoyama K, Kuroiwa Y, Hattori N, Okamoto T, Murata M, Toda T, Miyake S, Yamamura T, 2013. Plasmablasts as migratory IgG-producing cells in the pathogenesis of neuromyelitis optica. PloS One 8, e83036. 10.1371/journal.pone.0083036 [PubMed: 24340077]

Clements JD, Norton EB, 2018. The Mucosal Vaccine Adjuvant LT(R192G/L211A) or dmLT. mSphere 3, e00215–18. 10.1128/mSphere.00215-18 [PubMed: 30045966]

Corbett KS, Nason MC, Flach B, Gagne M, O'Connell S, Johnston TS, Shah SN, Edara VV, Floyd K, Lai L, McDanal C, Francica JR, Flynn B, Wu K, Choi A, Koch M, Abiona OM, Werner AP, Moliva JI, Andrew SF, Donaldson MM, Fintzi J, Flebbe DR, Lamb E, Noe AT, Nurmukhambetova ST, Provost SJ, Cook A, Dodson A, Faudree A, Greenhouse J, Kar S, Pessaint L, Porto M, Steingrebe K, Valentin D, Zouantcha S, Bock KW, Minai M, Nagata BM, van de Wetering R, Boyoglu-Barnum S, Leung K, Shi W, Yang ES, Zhang Y, Todd J-PM, Wang L, Alvarado GS, Andersen H, Foulds KE, Edwards DK, Mascola JR, Moore IN, Lewis MG, Carfi A, Montefiori D, Suthar MS, McDermott A, Roederer M, Sullivan NJ, Douek DC, Graham BS, Seder RA, 2021. Immune correlates of protection by mRNA-1273 vaccine against SARS-CoV-2 in nonhuman primates. Science 373. 10.1126/science.abj0299

Dando SJ, Mackay-Sim A, Norton R, Currie BJ, St John JA, Ekberg JAK, Batzloff M, Ulett GC, Beacham IR, 2014. Pathogens penetrating the central nervous system: infection pathways and the cellular and molecular mechanisms of invasion. Clin. Microbiol. Rev 27, 691–726. 10.1128/CMR.00118-13 [PubMed: 25278572]

de Melo GD, Lazarini F, Levallois S, Hautefort C, Michel V, Larrous F, Verillaud B, Aparicio C, Wagner S, Gheusi G, Kergoat L, Kornobis E, Donati F, Cokelaer T, Hervochon R, Madec Y, Roze E, Salmon D, Bourhy H, Lecuit M, Lledo P-M, 2021. COVID-19-related anosmia is associated with viral persistence and inflammation human olfactory epithelium and brain infection in hamsters. Sci. Transl. Med 13, eabf8396. 10.1126/scitranslmed.abf8396 [PubMed: 33941622]

Dieterle ME, Haslwanter D, Bortz RH, Wirchnianski AS, Lasso G, Vergnolle O, Abbasi SA, Fels JM, Laudermilch E, Florez C, Mengotto A, Kimmel D, Malonis RJ, Georgiev G, Quiroz J,

Barnhill J, Pirofski L, Daily JP, Dye JM, Lai JR, Herbert AS, Chandran K, Jangra RK, 2020. A Replication-Competent Vesicular Stomatitis Virus for Studies of SARS-CoV-2 Spike-Mediated Cell Entry and Its Inhibition. Cell Host Microbe 28, 486–496.e6. 10.1016/j.chom.2020.06.020 [PubMed: 32738193]

Duckworth BC, Lafouresse F, Wimmer VC, Broomfield BJ, Dalit L, Alexandre YO, Sheikh AA, Qin RZ, Alvarado C, Mielke LA, Pellegrini M, Mueller SN, Boudier T , Rogers KL, Groom JR, 2021. Effector and stem-like memory cell fates are imprinted in distinct lymph node niches directed by CXCR3 ligands. Nat. Immunol 22, 434–448. 10.1038/s41590-021-00878-5 [PubMed: 33649580]

Dumm RE, Fiege JK, Waring BM, Kuo CT, Langlois RA, Heaton NS, 2019. Non-lytic clearance of influenza B virus from infected cells preserves epithelial barrier function. Nat. Commun 10, 779. 10.1038/s41467-019-08617-z [PubMed: 30770807]

Dumm RE, Wellford SA, Moseman EA, Heaton NS, 2020. Heterogeneity of Antiviral Responses in the Upper Respiratory Tract Mediates Differential Non-lytic Clearance of Influenza Viruses. Cell Rep. 32, 108103. 10.1016/j.celrep.2020.108103 [PubMed: 32877682]

Durante MA, Kurtenbach Stefan, Sargi ZB, Harbour JW, Choi R, Kurtenbach Sarah, Goss GM, Matsunami H, Goldstein BJ, 2020. Single-cell analysis of olfactory neurogenesis and differentiation in adult humans. Nat. Neurosci 23, 323–326. 10.1038/s41593-020-0587-9 [PubMed: 32066986]

Fehervari Z, 2021. Intranasal vaccination. Nat. Immunol 22, 1071–1071. 10.1038/s41590-021-01016-x

Field-Smith A, Morgan GJ, Davies FE, 2006. Bortezomib (Velcade™) in the Treatment of Multiple Myeloma. Ther. Clin. Risk Manag 2, 271–279. [PubMed: 18360602]

Fitzpatrick Z, Frazer G, Ferro A, Clare S, Bouladoux N, Ferdinand J, Tuong ZK, Negro-Demontel ML, Kumar N, Suchanek O, Tajsic T, Harcourt K, Scott K, Bashford-Rogers R, Helmy A, Reich DS, Belkaid Y, Lawley TD, McGavern DB, Clatworthy MR, 2020. Gut-educated IgA plasma cells defend the meningeal venous sinuses. Nature, 10.1038/s41586-020-2886-4

Fröberg J, Gillard J, Philipsen R, Lanke K, Rust J, van Tuijl D, Teelen K, Bousema T, Simonetti E, van der Gaast-de Jongh CE, Bos M, van Kuppeveld FJ, Bosch B-J, Nabuurs-Franssen M, van der Geest-Blankert N, van Daal C, Huynen MA, de Jonge MI, Diavatopoulos DA, 2021. SARS-CoV-2 mucosal antibody development and persistence and their relation to viral load and COVID-19 symptoms. Nat. Commun 12, 5621. 10.1038/s41467-021-25949-x [PubMed: 34556667]

Fumagalli V, Ravà M, Marotta D, Lucia PD, Laura C, Sala E, Grillo M, Bono E, Giustini L, Perucchini C, Mainetti M, Sessa A, Garcia-Manteiga JM, Donnici L, Manganaro L, Delbue S, Broccoli V, Francesco RD, D'Adamo P, Kuka M, Guidotti LG, Iannacone M, 2021. Administration of aerosolized SARS-CoV-2 to K18-hACE2 mice uncouples respiratory infection from fatal neuroinvasion. Sci. Immunol 10.1126/sciimmunol.abl9929

Glauser DL, Milho R, Lawler C, Stevenson PG, 2019. Antibody arrests γ-herpesvirus olfactory super-infection independently of neutralization. J. Gen. Virol 100, 246–258. 10.1099/jgv.0.001183 [PubMed: 30526737]

Green PA, Van Valkenburgh B, Pang B, Bird D, Rowe T, Curtis A, 2012. Respiratory and olfactory turbinal size in canid and arctoid carnivorans. J. Anat 221, 609–621. 10.1111/j.1469-7580.2012.01570.x [PubMed: 23035637]

Groom JR, Luster AD, 2011. CXCR3 ligands: Redundant, collaborative and antagonistic functions. Immunol. Cell Biol 89, 207–215. 10.1038/icb.2010.158 [PubMed: 21221121]

Groom JR, Richmond J, Murooka TT, Sorensen EW, Sung JH, Bankert K, von Andrian UH, Moon JJ, Mempel TR, Luster AD, 2012. CXCR3 chemokine receptor-ligand interactions in the lymph node optimize CD4+ T helper 1 cell differentiation. Immunity 37, 1091–1103. 10.1016/j.immuni.2012.08.016 [PubMed: 23123063]

Hassan AO, Kafai NM, Dmitriev IP, Fox JM, Smith BK, Harvey IB, Chen RE, Winkler ES, Wessel AW, Case JB, Kashentseva E, McCune BT, Bailey AL, Zhao H, VanBlargan LA, Dai YN, Ma M, Adams LJ, Shrihari S, Danis JE, Gralinski LE, Hou YJ, Schäfer A, Kim AS, Keeler SP, Weiskopf D, Baric RS, Holtzman MJ, Fremont DH, Curiel DT, Diamond MS, 2020. A Single-Dose Intranasal ChAd Vaccine Protects Upper and Lower Respiratory Tracts against SARS-CoV-2. Cell 183, 169–184.e13. 10.1016/j.cell.2020.08.026 [PubMed: 32931734]

Hauser AE, Debes GF, Arce S, Cassese G, Hamann A, Radbruch A, Manz RA, 2002. Chemotactic responsiveness toward ligands for CXCR3 and CXCR4 is regulated on plasma blasts during the

time course of a memory immune response. J. Immunol. Baltim. Md 1950 169, 1277–1282. 10.4049/jimmunol.169.3.1277

Horiuchi S, Oishi K, Carrau L, Frere J, Møller R, Panis M, tenOever BR, 2021. Immune memory from SARS-CoV-2 infection in hamsters provides variant-independent protection but still allows virus transmission. Sci. Immunol 10.1126/sciimmunol.abm3131

Horton RE, Vidarsson G, 2013. Antibodies and their receptors: Different potential roles in mucosal defense. Front. Immunol 4. 10.3389/fimmu.2013.00200

Hura N, Xie DX, Choby GW, Schlosser RJ, Orlov CP, Seal SM, Rowan NR, 2020. Treatment of post-viral olfactory dysfunction: an evidence-based review with recommendations. Int. Forum Allergy Rhinol 10, 1065–1086. 10.1002/alr.22624 [PubMed: 32567798]

Iannacone M, Moseman EA, Tonti E, Bosurgi L, Junt T, Henrickson SE, Whelan SP, Guidotti LG, von Andrian UH, 2010. Subcapsular sinus macrophages prevent CNS invasion on peripheral infection with a neurotropic virus. Nature 465, 1079–1083. 10.1038/nature09118 [PubMed: 20577213]

Iijima N, Iwasaki A, 2016. Access of protective antiviral antibody to neuronal tissues requires CD4 T-cell help. Nature 533, 552–556. 10.1038/naturel7979 [PubMed: 27225131]

Iwasaki A, 2017. Immune Regulation of Antibody Access to Neuronal Tissues. Trends Mol. Med 23, 227–245. 10.1016/j.molmed.2017.01.004 [PubMed: 28185790]

Jang H, Boltz D, Sturm-Ramirez K, Shepherd KR, Jiao Y, Webster R, Smeyne RJ, 2009. Highly pathogenic H5N1 influenza virus can enter the central nervous system and induce neuroinflammation and neurodegeneration. Proc. Natl. Acad. Sci. U. S. A 106, 14063–14068. 10.1073/pnas.0900096106 [PubMed: 19667183]

Johnson JL, Rosenthal RL, Knox JJ, Myles A, Naradikian MS, Madej J, Kostiv M, Rosenfeld AM, Meng W, Christensen SR, Hensley SE, Yewdell J, Canaday DH, Zhu J, McDermott AB, Dori Y, Itkin M, Wherry EJ, Pardi N, Weissman D, Naji A, Prak ETL, Betts MR, Cancro MP, 2020. The Transcription Factor T-bet Resolves Memory B Cell Subsets with Distinct Tissue Distributions and Antibody Specificities in Mice and Humans. Immunity 52, 842–855.e6. 10.1016/j.immuni.2020.03.020 [PubMed: 32353250]

Kalinke U, Bucher EM, Ernst B, Oxenius A, Roost H-P, Geley S, Kofler R, Zinkernagel RM, Hengartner H, 1996. The Role of Somatic Mutation in the Generation of the Protective Humoral Immune Response against Vesicular Stomatitis Virus. Immunity 5, 639–652. 10.1016/S1074-7613(00)80277-0 [PubMed: 8986722]

Kato A, Hulse KE, Tan BK, Schleimer RP, 2013. B-lymphocyte lineage cells and the respiratory system. J. Allergy Clin. Immunol 131, 933–957. 10.1016/j.jaci.2013.02.023 [PubMed: 23540615]

Keller B, Strohmeier V, Harder I, Unger S, Payne KJ, Andrieux G, Boerries M, Felixberger PT, Landry JJM, Nieters A, Rensing-Ehl A, Salzer U, Frede N, Usadel S , Elling R, Speckmann C, Hainmann I, Ralph E, Gilmour K, Wentink MWJ, van der Burg M, Kuehn HS, Rosenzweig SD, Kölsch U, von Bernuth H, Kaiser-Labusch P, Gothe F, Hambleton S, Vlagea AD, Garcia Garcia A, Alsina L, Markelj G, Avcin T , Vasconcelos J, Guedes M, Ding J-Y, Ku C-L, Shadur B, Avery DT, Venhoff N, Thiel J, Becker H, Erazo-Borrás L, Trujillo-Vargas CM, Franco JL, Fieschi C, Okada S, Gray PE, Uzel G, Casanova J-L, Fliegauf M, Grimbacher B, Eibel H, Ehl S, Voll RE, Rizzi M, Stepensky P, Benes V, Ma CS, Bossen C, Tangye SG, Warnatz K, 2021. The expansion of human T-bethighCD21low B cells is T cell dependent. Sci. Immunol 6, eabh0891. 10.1126/sciimmunol.abh0891 [PubMed: 34623902]

Khan M, Yoo S-J, Clijsters M, Backaert W, Vanstapel A, Speleman K, Lietaer C, Choi S, Hether TD, Marcelis L, Nam A, Pan L, Reeves JW, Van Bulck P, Zhou H, Bourgeois M, Debaveye Y, De Munter P, Gunst J, Jorissen M, Lagrou K, Lorent N, Neyrinck A, Peetermans M, Thal DR, Vandenbriele C, Wauters J, Mombaerts P, Van Gerven L, 2021. Visualizing in deceased COVID-19 patients how SARS-CoV-2 attacks the respiratory and olfactory mucosae but spares the olfactory bulb. Cell S0092-8674(21)01282–4. 10.1016/j.cell.2021.10.027

Kumar NN, Lochhead JJ, Pizzo ME, Nehra G, Boroumand S, Greene G, Thorne RG, 2018. Delivery of immunoglobulin G antibodies to the rat nervous system following intranasal administration: Distribution, dose-response, and mechanisms of delivery. J. Controlled Release 286, 467–484. 10.1016/j.jconrel.2018.08.006

Lavelle EC, Ward RW, 2021. Mucosal vaccines — fortifying the frontiers. Nat. Rev. Immunol 1–15. 10.1038/s41577-021-00583-2 [PubMed: 33303954]

Lawler C, Stevenson PG, 2017. Type I Interferon Signaling to Dendritic Cells Limits Murid Herpesvirus 4 Spread from the Olfactory Epithelium. J. Virol 91, e00951–17. 10.1128/JVI.00951-17 [PubMed: 28904198]

Lee N, Wong CK, Chan PKS, Lindegardh N, White NJ, Hayden FG, Wong EHC, Wong KS, Cockram CS, Sung JJY, Hui DSC, 2010. Acute Encephalopathy Associated with Influenza A Infection in Adults. Emerg. Infect. Dis 16, 139–142. 10.3201/eidl601.090077 [PubMed: 20031062]

Lefrancois L, 1984. Protection against lethal viral infection by neutralizing and nonneutralizing monoclonal antibodies: distinct mechanisms of action in vivo. J. Virol 51, 208–214. 10.1128/JVI.51.l.208-214.1984 [PubMed: 6328040]

Lemke A, Kraft M, Roth K, Riedel R, Lammerding D, Hauser AE, 2016. Long-lived plasma cells are generated in mucosal immune responses and contribute to the bone marrow plasma cell pool in mice. Mucosal Immunol. 9, 83–97. 10.1038/mi.2015.38 [PubMed: 25943272]

Lightman SM, Utley A, Lee KP, 2019. Survival of long-lived plasma cells (LLPC): Piecing together the puzzle. Front. Immunol 10, 965–965. 10.3389/fimmu.2019.00965 [PubMed: 31130955]

Lochhead JJ, Thorne RG, 2012. Intranasal delivery of biologics to the central nervous system. Adv. Drug Deliv. Rev 64, 614–628. 10.1016/j.addr.2011.ll.002 [PubMed: 22119441]

Mades A, Chellamathu P, Kojima N, Lopez L, MacMullan MA, Denny N, Angel AN, Santacruz M, Casian JG, Brobeck M, Nirema N, Klausner JD, Turner F, Slepnev VI, Ibrayeva A, 2021. Detection of persistent SARS-CoV-2 IgG antibodies in oral mucosal fluid and upper respiratory tract specimens following COVID-19 mRNA vaccination. Sci. Rep 11, 24448. 10.1038/s41598-021-03931-3 [PubMed: 34961780]

Manning ML, Mason-Osann E, Onda M, Pastan I, 2015. Bortezomib reduces pre-existing antibodies to recombinant immunotoxins in mice. J. Immunol. Baltim. Md 1950 194, 1695–1701. 10.4049/jimmunol.1402324

Mantis NJ, Rol N, Corthésy B, 2011. Secretory IgA's complex roles in immunity and mucosal homeostasis in the gut. Mucosal Immunol. 4, 603–611. 10.1038/mi.2011.41 [PubMed: 21975936]

Marques CP, Kapil P, Hinton DR, Hindinger C, Nutt SL, Ransohoff RM, Phares TW, Stohlman SA, Bergmann CC, 2011. CXCR3-dependent plasma blast migration to the central nervous system during viral encephalomyelitis. J. Virol 85, 6136–6147. 10.1128/JVI.00202-ll [PubMed: 21507985]

Martin V, Hoekman J, Aurora SK, Shrewsbury SB, 2021. Nasal Delivery of Acute Medications for Migraine: The Upper Versus Lower Nasal Space. J. Clin. Med 10, 2468. 10.3390/jcml0112468 [PubMed: 34199479]

Mazanec MB, Nedrud JG, Liang XP, Lamm ME, 1989. Transport of serum IgA into murine respiratory secretions and its implications for immunization strategies. J. Immunol 142, 4275–4281. [PubMed: 2542407]

McCullers JA, Facchini S, Chesney PJ, Webster RG, 1999. Influenza B virus encephalitis - PubMed [WWW Document]. URL https://pubmed.ncbi.nlm.nih.gov/10825057/ (accessed 3.23.22).

McMahan K, Yu J, Mercado NB, Loos C, Tostanoski LH, Chandrashekar A, Liu J, Peter L, Atyeo C, Zhu A, Bondzie EA, Dagotto G, Gebre MS, Jacob-Dolan C, Li Z, Nampanya F, Patel S, Pessaint L, Van Ry A, Blade K, Yalley-Ogunro J, Cabus M, Brown R, Cook A, Teow E, Andersen H, Lewis MG, Lauffenburger DA, Alter G, Barouch DH, 2021. Correlates of protection against SARS-CoV-2 in rhesus macaques. Nature 590, 630–634. 10.1038/s41586-020-03041-6 [PubMed: 33276369]

Mei HE, Wirries I, Frölich D, Brisslert M, Giesecke C, Grün JR, Alexander T, Schmidt S, Luda K, Kühl AA, Engelmann R, Dürr M, Scheel T, Bokarewa M, Perka C, Radbruch A, Dörner T, 2015. A unique population of IgG-expressing plasma cells lacking CD19 is enriched in human bone marrow. Blood 125, 1739–1748. 10.1182/blood-2014-02-555169 [PubMed: 25573986]

Mellert TK, Getchell ML, Sparks L, Getchell TV, 1991. Characterization of the immune barrier in human olfactory mucosa.

Meng X, Deng Y, Dai Z, Meng Z, 2020. COVID-19 and anosmia: A review based on up-to-date knowledge. Am. J. Otolaryngol. - Head Neck Med. Surg 41, 102581–102581. 10.1016/j.amjoto.2020.102581

Mori E, Ueha R, Kondo K, Funada S, Shimmura H, Kanemoto K, Tanaka H, Nishijima H, Otori N, Yamasoba T, Kojima H, 2021. Squamous and Respiratory Metaplasia After Olfactory Mucosal Resection. Front. Neurosci 15.

Mori I, 2018. Highlighting the “blood-nerve barrier” in virology research. Acta Virol. 62, 28–32. 10.4149/av_2018_103 [PubMed: 29521100]

Moseman EA, 2020. Battling brain-eating amoeba: Enigmas surrounding immunity to Naegleria fowleri. PLOS Pathog. 16, e1008406. 10.1371/journal.ppat.1008406 [PubMed: 32324819]

Moseman EA, Blanchard AC, Nayak D, McGavern DB, 2020. T cell engagement of cross-presenting microglia protects the brain from a nasal virus infection. Sci. Immunol 5, eabb1817–eabb1817. 10.1126/sciimmunol.abbl817 [PubMed: 32503876]

Moseman EA, Iannacone M, Bosurgi L, Tonti E, Chevrier N, Tumanov A, Fu Y-X, Hacohen N, von Andrian UH, 2012. B cell maintenance of subcapsular sinus macrophages protects against a fatal viral infection independent of adaptive immunity. Immunity 36, 415–26. 10.1016/j.immuni.2012.01.013 [PubMed: 22386268]

Muehlinghaus G, Cigliano L, Huehn S, Peddinghaus A, Leyendeckers H, Hauser AE, Hiepe F, Radbruch A, Arce S, Manz RA, 2005. Regulation of CXCR3 and CXCR4 expression during terminal differentiation of memory B cells into plasma cells. Blood 105, 3965–3971. 10.1182/BLOOD-2004-08-2992 [PubMed: 15687242]

Müller M, Carter S, Hofer MJ, Campbell IL, 2010. Review: The chemokine receptor CXCR3 and its ligands CXCL9, CXCL10 and CXCL11 in neuroimmunity--a tale of conflict and conundrum. Neuropathol. Appl. Neurobiol 36, 368–387. 10.1111/j.1365-2990.2010.01089.x [PubMed: 20487305]

Muramatsu M, Kinoshita K, Fagarasan S, Yamada S, Shinkai Y, Honjo T, 2000. Class Switch Recombination and Hypermutation Require Activation-Induced Cytidine Deaminase (AID), a Potential RNA Editing Enzyme. Cell 102, 553–563. 10.1016/S0092-8674(00)00078-7 [PubMed: 11007474]

Muzumdar MD, Tasic B, Miyamichi K, Li L, Luo L, 2007. A global double-fluorescent Cre reporter mouse. Genes. N. Y. N 2000 45, 593–605. 10.1002/dvg.20335

Naradikian MS, Myles A, Beiting DP, Roberts KJ, Dawson L, Herati RS, Bengsch B, Linderman SL, Stelekati E, Spolski R, Wherry EJ, Hunter C, Hensley SE, Leonard WJ, Cancro MP, 2016. IL4, IL21, and IFNγ interact to govern TBET and CD11c expression in TLR-activated B cells. J. Immunol. Baltim. Md 1950 197, 1023–1028. 10.4049/jimmunol.1600522

Neubert K, Meister S, Moser K, Weisel F, Maseda D, Amann K, Wiethe C, Winkler TH, Kalden JR, Manz RA, Voll RE, 2008. The proteasome inhibitor bortezomib depletes plasma cells and protects mice with lupus-like disease from nephritis. Nat. Med 14, 748–755. 10.1038/nml763 [PubMed: 18542049]

Newland JG, Romero JR, Varman M, Drake C, Holst A, Safranek T, Subbarao K, 2003. Encephalitis Associated with Influenza B Virus Infection in 2 Children and a Review of the Literature. Clin. Infect. Dis 36, e87–e95. 10.1086/368184 [PubMed: 12652406]

Nie Y, Waite J, Brewer F, Sunshine M-J, Litttman DR, Zou Y-R, 2004. The role of CXCR4 in maintaining peripheral B cell compartments and humoral immunity. J. Exp. Med

Niimi K, Usami K, Fujita Y, Abe M, Furukawa M, Suyama Y, Sakai Y, Kamioka M, Shibata N, Park EJ, Sato S, Kiyono H, Yoneyama H, Kitazawa H, Watanabe K, Nochi T, Aso H, 2018. Development of immune and microbial environments is independently regulated in the mammary gland. Mucosal Immunol. 11, 643–653. 10.1038/mi.2017.90 [PubMed: 29346344]

Oberland S, Neuhaus EM, 2014. Whole mount labeling of cilia in the main olfactory system of mice. J. Vis. Exp. JoVE 10.3791/52299

Oh JE, Iijima N, Song E, Lu P, Klein J, Jiang R, Kleinstein SH, Iwasaki A, 2019. Migrant memory B cells secrete luminal antibody in the vagina. Nature 571, 122–126. 10.1038/s41586-019-1285-l [PubMed: 31189952]

Oh JE, Song E, Moriyama M, Wong P, Zhang S, Jiang R, Strohmeier S, Kleinstein SH, Krammer F, Iwasaki A, 2021. Intranasal priming induces local lung-resident B cell populations that secrete protective mucosal antiviral IgA. Sci. Immunol 10.1126/sciimmunol.abj5129

Paik SI, Lehman MN, Seiden AM, Duncan HJ, Smith DV, 1992. Human Olfactory Biopsy: The Influence of Age and Receptor Distribution. Arch. Otolaryngol. Neck Surg 118, 731–738. 10.1001/archotol.1992.01880070061012

Pakkanen SH, Kantele JM, Moldoveanu Z, Hedges S, Häkkinen M, Mestecky J, Kantele A, 2010. Expression of homing receptors on IgA1 and IgA2 plasmablasts in blood reflects differential distribution of IgA1 and IgA2 in various body fluids. Clin. Vaccine Immunol 17, 393–401. 10.1128/CVI.00475-09 [PubMed: 20089794]

Pilette C, Ouadrhiri Y, Godding V, Vaerman J-P, Sibille Y, 2001. Lung mucosal immunity: immunoglobulin-A revisited. Eur. Respir. J 18, 571–588. [PubMed: 11589357]

Plourde JR, Pyles JA, Layton RC, Vaughan SE, Tipper JL, Harrod KS, 2012. Neurovirulence of H5N1 infection in ferrets is mediated by multifocal replication in distinct permissive neuronal cell regions. PloS One 7, e46605. 10.1371/journal.pone.0046605 [PubMed: 23056366]

Polack FP, Thomas SJ, Kitchin N, Absalon J, Gurtman A, Lockhart S, Perez JL, Pérez Marc G, Moreira ED, Zerbini C, Bailey R, Swanson KA, Roychoudhury S, Koury K, Li P, Kalina WV, Cooper D, Frenck RW, Hammitt LL, Türeci Ö, Nell H, Schaefer A, Ünal S, Tresnan DB, Mather S, Dormitzer PR, Şahin U, Jansen KU, Gruber WC, 2020. Safety and Efficacy of the BNT162b2 mRNA Covid-19 Vaccine. N. Engl. J. Med 383, 2603–2615. 10.1056/NEJMoa2034577 [PubMed: 33301246]

Popescu CP, Florescu SA, Lupulescu E, Zaharia M, Tardei G, Lazar M, Ceausu E, Ruta SM, 2017. Neurologic Complications of Influenza B Virus Infection in Adults, Romania. Emerg. Infect. Dis 23, 574–581. 10.3201/eid2304.161317 [PubMed: 28322689]

Premraj L, Kannapadi NV, Briggs J, Seal SM, Battaglini D, Fanning J, Suen J, Robba C, Fraser J, Cho S-M, 2022. Mid and long-term neurological and neuropsychiatric manifestations of post-COVID-19 syndrome: A meta-analysis. J. Neurol. Sci 434, 120162. 10.1016/j.jns.2022.120162 [PubMed: 35121209]

Reiss CS, PLAKHOV IV, KOMATSU T, 1998. Viral Replication in Olfactory Receptor Neurons and Entry into the Olfactory Bulb and Brain. Ann. N. Y. Acad. Sci 855, 751–761. 10.1111/j.1749-6632.1998.tbl0655.x [PubMed: 9929681]

Renaud M, Thibault C, Le Normand F, Mcdonald EG, Gallix B, Debry C, Venkatasamy A, 2021. Clinical Outcomes for Patients With Anosmia 1 Year After COVID-19 Diagnosis. JAMA Netw. Open 4, e2115352. 10.1001/jamanetworkopen.2021.15352 [PubMed: 34165581]

Renegar KB, Small PA, 1994. Immunization: Systemic and Mucosal. Handb. Mucosal Immunol 347–356.

Renegar KB, Small PA, Boykins LG, Wright PF, 2004. Role of IgA versus IgG in the Control of Influenza Viral Infection in the Murine Respiratory Tract. J. Immunol 173, 1978–1986. 10.4049/jimmunol.173.3.1978 [PubMed: 15265932]

Reyes C, Miranda S, Fica A, Navarrete M, 2019. [Encephalitis caused by type B influenza virus in an adult. Report of one case]. Rev. Med. Chil 147, 922–927. 10.4067/S0034-98872019000700922 [PubMed: 31859991]

Rosenthal KL, Zinkernagel RM, 1980. Cross-reactive cytotoxic T cells to serologically distinct vesicular stomatitis virus. J. Immunol. Baltim. Md 1950 124, 2301–2308.

Schrauwen EJA, Herfst S, Leijten LM, van Run P, Bestebroer TM, Linster M, Bodewes R, Kreijtz JHCM, Rimmelzwaan GF, Osterhaus ADME, Fouchier RAM, Kuiken T, van Riel D, 2012. The multibasic cleavage site in H5N1 virus is critical for systemic spread along the olfactory and hematogenous routes in ferrets. J. Virol 86, 3975–3984. 10.1128/JVI.06828-ll [PubMed: 22278228]

Scott DW, Gershon RK, 1970. Determination of total and merecaptothanol-resistant antibody in the same serum sample. Clin. Exp. Immunol 6, 313–316. [PubMed: 5435721]

Serre K, Cunningham AF, Coughlan RE, Lino AC, Rot A, Hub E, Moser K, Manz R, Ferraro A, Bird R, Toellner K-M, Demengeot J, MacLennan ICM, Mohr E, 2012. CD8 T cells induce T-bet–dependent migration toward CXCR3 ligands by differentiated B cells produced during responses to alum-protein vaccines. Blood 120, 4552–4559. 10.1182/blood-2012-03-417733 [PubMed: 23065152]

Sheikh-Mohamed S, Chao GYC, Isho B, Zuo M, Nahass GR, Salomon-Shulman RE, Blacker G, Fazel-Zarandi M, Rathod B, Colwill K, Jamal A, Li Z, Launay K.Q. de, Takaoka A, Garnham-Takaoka J, Fahim C, Paterson A, Li AX, Haq N, Barati S, Gilbert L, Green K, Mozafarihashjin M, Samaan P, Siqueira WL, Mubareka S, Ostrowski M, Rini JM, Rojas OL, McGeer A, Weissman IL, Tal MC, Straus S, Gingras A-C, Gommerman JL, 2021. A mucosal antibody response is induced by intramuscular SARS-CoV-2 mRNA vaccination, 10.1101/2021.08.01.21261297

Shin H, Iwasaki A, 2012. A vaccine strategy protects against genital herpes by establishing local memory T cells. Nature 491, 463–467. 10.1038/naturell522 [PubMed: 23075848]

Shivkumar M, Milho R, May JS, Nicoll MP, Efstathiou S, Stevenson PG, 2013. Herpes simplex virus 1 targets the murine olfactory neuroepithelium for host entry. J. Virol 87, 10477–88. 10.1128/JVI.01748-13 [PubMed: 23903843]

Song W, Antao OQ, Condiff E, Sanchez GM, Chernova I, Zembrzuski K, Steach H, Rubtsova K, Angeletti D, Lemenze A, Laidlaw BJ, Craft J, Weinstein JS, 2022. Development of Tbet- and CD11c-expressing B cells in a viral infection requires T follicular helper cells outside of germinal centers. Immunity 55, 290–307.e5. 10.1016/j.immuni.2022.01.002 [PubMed: 35090581]

Steininger C, Popow-Kraupp T, Laferl H, Seiser A, Gödl I Djamshidian S, Puchhammer-Stöckl E, 2003. Acute encephalopathy associated with influenza A virus infection. Clin. Infect. Dis. Off. Publ. Infect. Dis. Soc. Am 36, 567–574. 10.1086/367623

Subbarao K, McAuliffe J, Vogel L, Fahle G, Fischer S, Tatti K, Packard M, Shieh W-J, Zaki S, Murphy B, 2004. Prior Infection and Passive Transfer of Neutralizing Antibody Prevent Replication of Severe Acute Respiratory Syndrome Coronavirus in the Respiratory Tract of Mice. J. Virol 78, 3572–3577. 10.1128/jvi.78.7.3572-3577.2004 [PubMed: 15016880]

Sung JH, Zhang H, Moseman EA, Alvarez D, Iannacone M, Henrickson SE, de la Torre JC, Groom JR, Luster AD, von Andrian UH, 2012. Chemokine Guidance of Central Memory T Cells Is Critical for Antiviral Recall Responses in Lymph Nodes. Cell 150, 1249–1263. 10.1016/j.cell.2012.08.015 [PubMed: 22980984]

Tan H-X, Juno JA, Esterbauer R, Kelly HG, Wragg KM, Konstandopoulos P, Alcantara S, Alvarado C, Jones R, Starkey G, Wang BZ, Yoshino O, Tiang T, Grayson ML, Opdam H, D'Costa R, Vago A, Group, the A.L.T.P., Mackay LK, Gordon CL, Masopust D, Groom JR, Kent SJ, Wheatley AK, 2022. Lung-resident memory B cells established after pulmonary influenza infection display distinct transcriptional and phenotypic profiles. Sci. Immunol 10.1126/sciimmunol.abf5314

Terreri S, Piano Mortari E, Vinci MR, Russo C, Alteri C, Albano C, Colavita F, Gramigna G, Agrati C, Linardos G, Coltella L, Colagrossi L, Deriu G, Ciofi Degli Atti M, Rizzo C, Scarsella M, Brugaletta R, Camisa V, Santoro A, Roscilli G, Pavoni E, Muzi A, Magnavita N, Scutari R, Villani A, Raponi M, Locatelli F, Perno CF, Zaffina S, Carsetti R, 2022. Persistent B cell memory after SARS-CoV-2 vaccination is functional during breakthrough infections. Cell Host Microbe 30, 400–408.e4. 10.1016/j.chom.2022.01.003 [PubMed: 35134333]

van den Brand JMA, Stittelaar KJ, van Amerongen G, Reperant L, de Waal L, Osterhaus ADME, Kuiken T, 2012. Comparison of temporal and spatial dynamics of seasonal H3N2, pandemic H1N1 and highly pathogenic avian influenza H5N1 virus infections in ferrets. PloS One 7, e42343. 10.1371/journal.pone.0042343 [PubMed: 22905124]

van der Feltz MJ, de Groot N, Bayley JP, Lee SH, Verbeet MP, de Boer HA, 2001. Lymphocyte homing and Ig secretion in the murine mammary gland. Scand. J. Immunol 54, 292–300. 10.1046/j.1365-3083.2001.00933.x [PubMed: 11555393]

van Doremalen N, Lambe T, Spencer A, Belij-Rammerstorfer S, Purushotham JN, Port JR, Avanzato VA, Bushmaker T, Flaxman A, Ulaszewska M, Feldmann F, Allen ER, Sharpe H, Schulz J, Holbrook M, Okumura A, Meade-White K, Pérez-Pérez L, Edwards NJ, Wright D, Bissett C, Gilbride C, Williamson BN, Rosenke R, Long D, Ishwarbhai A, Kailath R, Rose L, Morris S, Powers C, Lovaglio J, Hanley PW, Scott D, Saturday G, de Wit E, Gilbert SC, Munster VJ, 2020. ChAdOx1 nCoV-19 vaccine prevents SARS-CoV-2 pneumonia in rhesus macaques. Nature 586, 578–582. 10.1038/s41586-020-2608-y [PubMed: 32731258]

Van Raemdonck K, Van den Steen PE, Liekens S, Van Damme J, Struyf S, 2015. CXCR3 ligands in disease and therapy. Cytokine Growth Factor Rev. 26, 311–327. 10.1016/j.cytogfr.2014.ll.009 [PubMed: 25498524]

Wagner DK, Clements ML, Reimer CB, Snyder M, Nelson DL, Murphy BR, 1987. Analysis of immunoglobulin G antibody responses after administration of live and inactivated influenza A vaccine indicates that nasal wash immunoglobulin G is a transudate from serum. J. Clin. Microbiol 25, 559–562. [PubMed: 3571460]

Weisel NM, Joachim SM, Smita S, Callahan D, Eisner RA, Conter LJ, Chikina M, Farber DL, Weisel FJ, Shlomchik MJ, 2022. Surface phenotypes of naive and memory B cells in mouse and human tissues. Nat. Immunol 23, 135–145. 10.1038/s41590-021-01078-x [PubMed: 34937918]

Weisel NM, Weisel FJ, Farber DL, Borghesi LA, Shen Y, Ma W, Luning Prak ET, Shlomchik MJ, 2020. Comprehensive analyses of B-cell compartments across the human body reveal novel subsets and a gut-resident memory phenotype. Blood 136, 2774–2785. 10.1182/blood.2019002782 [PubMed: 32750113]

Wright DE, Wagers AJ, Gulati AP, Johnson FL, Weissman IL, 2001. Physiological migration of hematopoietic stem and progenitor cells. Science 294, 1933–1936. 10.1126/science.1064081 [PubMed: 11729320]

Xydakis MS, Albers MW, Holbrook EH, Lyon DM, Shih RY, Frasnelli JA, Pagenstecher A, Kupke A, Enquist LW, Perlman S, 2021. Post-viral effects of COVID-19 in the olfactory system and their implications. Lancet Neurol. 0. 10.1016/S1474-4422(21)00182-4

Yu Y-Y, Kong W, Yin Y-X, Dong F, Huang Z-Y, Yin G-M, Dong S, Salinas I, Zhang Y-A, Xu Z, 2018. Mucosal immunoglobulins protect the olfactory organ of teleost fish against parasitic infection. PLOS Pathog. 14, e1007251–e1007251. 10.1371/journal.ppat.1007251 [PubMed: 30395648]

Zheng J, Wong LYR, Li K, Verma AK, Ortiz M, Wohlford-Lenane C, Leidinger MR, Knudson CM, Meyerholz DK, McCray PB, Perlman S, 2020. COVID-19 treatments and pathogenesis including anosmia in K18-hACE2 mice. Nature. 10.1038/s41586-020-2943-z

Zhou D, Chan JF-W, Zhou B, Zhou R, Li S, Shan S, Liu L, Zhang AJ, Chen SJ, Chan CC-S, Xu H, Poon VK-M, Yuan S, Li C, Chik KK-H, Chan CC-Y, Cao J, Chan C-Y, Kwan K-Y, Du Z, Lau TT-K, Zhang Q, Zhou J, To KK-W, Zhang L, Ho DD, Yuen K-Y, Chen Z, 2021. Robust SARS-CoV-2 infection in nasal turbinates after treatment with systemic neutralizing antibodies. Cell Host Microbe 29, 551–563.e5. 10.1016/j.chom.2021.02.019 [PubMed: 33657424]

Zhou R, Caspi RR, 2010. Ocular immune privilege. F1000 Biol. Rep 2, 3. 10.3410/B2-3 [PubMed: 20948803]

Zhou S, Kurt-Jones EA, Fitzgerald KA, Wang JP, Cerny AM, Chan M, Finberg RW, 2007. Role of MyD88 in Route-Dependent Susceptibility to Vesicular Stomatitis Virus Infection. J. Immunol 178, 5173–5181. 10.4049/jimmunol.178.8.5173 [PubMed: 17404300]

Highlights

- The olfactory mucosa is not protected by serum antibody
- A blood-endothelial barrier separates olfactory mucosa from circulating antibody
- Mucosal plasma cells within olfactory tissue secrete local, protective antibody
- Vaccinations often fail to drive plasma cells to the olfactory mucosa

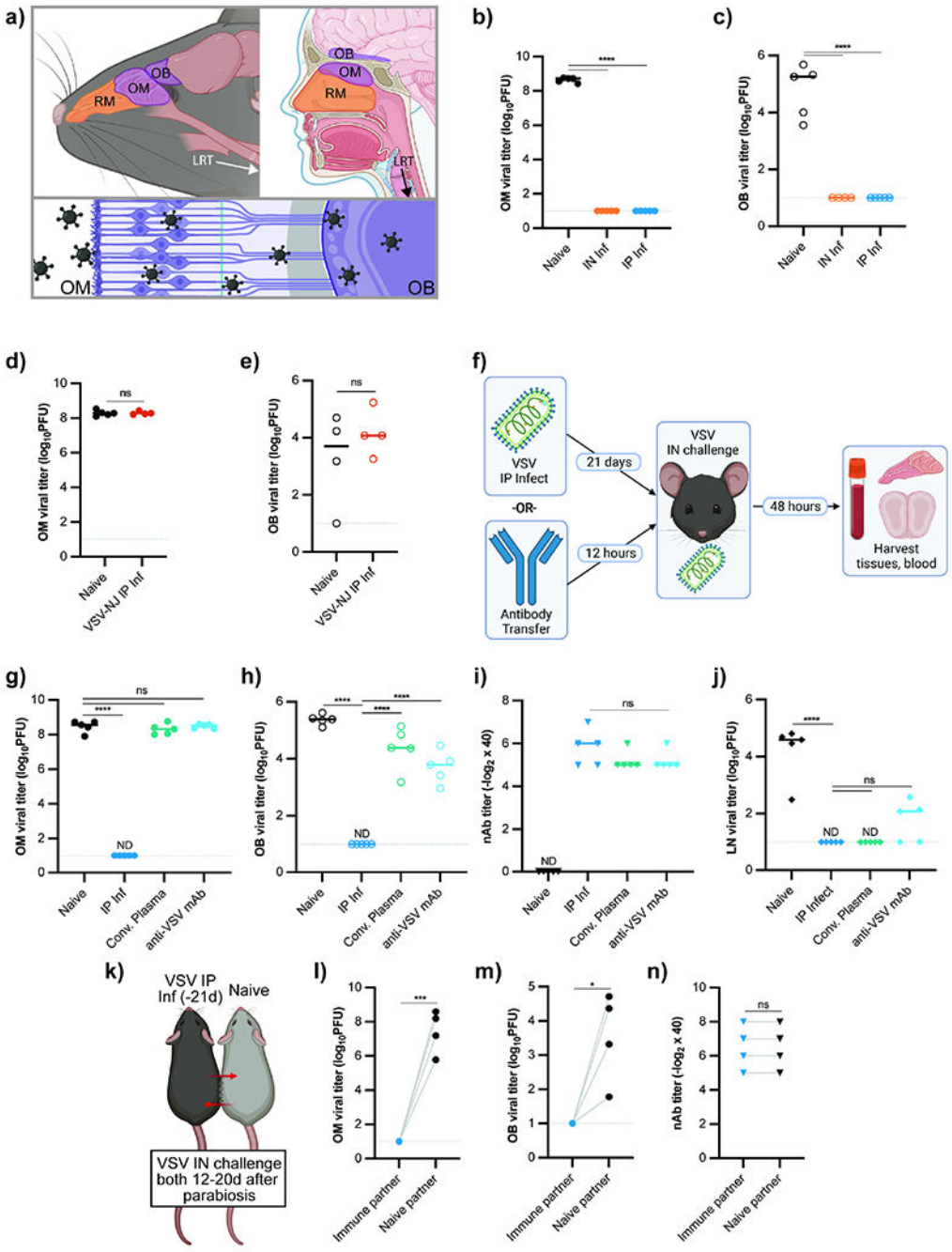

Figure 1 - Circulating Antibody Fails to Protect URT and Brain from Viral Infection

(a) Murine (left) and human (right) URT and brain, with olfactory regions in purple. Viral neuroinvasion via OSNs depicted below. **(b-c)** OM VSV titers **(b)** and OB VSV titers **(c)** from mice challenged IN with VSV. Experimental groups: naive mice (n = 5) and mice infected either IN (n = 5) or IP (n = 5) with VSV 35d prior to challenge. Data representative of two independent experiments. **(d-e)** OM VSV titers **(d)** and OB VSV titers **(e)** from mice IP infected with VSV-NJ and 28d later challenged IN with VSV-IND alongside naïve controls. **(f-i)** Experimental design **(f)**, OM VSV titers **(g)**, OB VSV titers **(h)**, and plasma

nAb titers **(i)**. Experimental groups: naïve mice (n = 5), mice IP infected with VSV 21d prior to IN rechallenge (n = 5), and mice receiving IP transfer of either α-VSV convalescent plasma (n = 5) or VI10 α-VSV monoclonal antibody (n = 5) 12h before VSV IN challenge. Data representative of two independent experiments. **(j)** LN VSV titers from mice treated as in (f-i) and challenged SC. Popliteal LNs harvested 8h after challenge. **(k-n)** Parabiosis experimental outline **(k)**, OM VSV titers **(l)**, OB VSV titers **(m)**, and plasma nAb titers **(n)**. Mice infected with VSV IP (−21d) were surgically conjoined with naïve mice. At either 12 (n = 2 pairs) or 20 (n = 2 pairs) days after attachment, both mice were challenged IN with VSV. For (b-c, g-j), statistical significance determined using Ordinary One-Way ANOVA with multiple comparisons. Parametric unpaired t-test used for (d-e). Ratio paired t-test used for (l-n). ND (not detected), ns (not significant) $P > 0.05$, * $P < 0.05$, ** $P < 0.01$, *** $P < 0.001$, **** $P < 0.0001$. See also Figure S1.

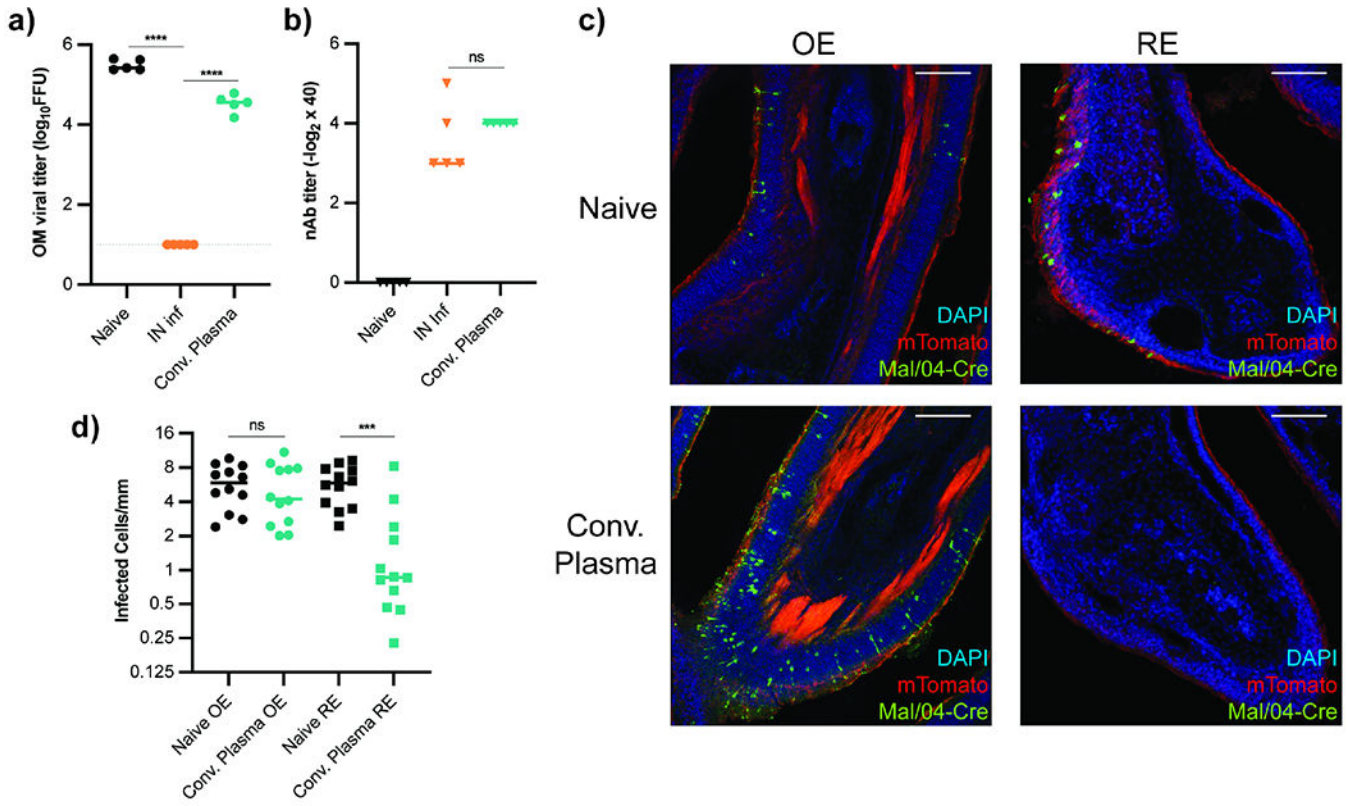

Figure 2 - Antibody Diifferentially Protects Nasal Respiratory and Olfactory Epithelium

(a-b) OM Mal/04 Influenza B viral titers **(a)** and plasma nAb titers **(b)** from IN infected mice. Experimental groups: mice infected with Mal/04 21d prior (n = 5), mice receiving anti-Mal/04 convalescent plasma (n = 5) 12h before challenge, and naïve mice (n = 5). Data representative of two independent experiments. **(c-d)** mT/mG mice were IN infected with Mal/04-Cre and fixed 48h later for immunofluorescent confocal microscopy. Mice received either no treatment (n = 4) or convalescent plasma transfer (n = 4) 12h prior to challenge. Representative images of OE and RE tissue shown in **(c)**. Quantification of infected cells (GFP+) per mm of epithelium, 3 sagittal sections per mouse **(d)**. Scale bars = 150 μm. Statistics in (a) calculated by ordinary One-Way ANOVA with multiple comparisons. Parametric unpaired t-test performed in (b). Comparisons in (d) evaluated using unpaired t-test with Welch's correction, ns (not significant) $P > 0.05$, * $P < 0.05$, ** $P < 0.01$, *** $P < 0.001$, **** $P < 0.0001$.

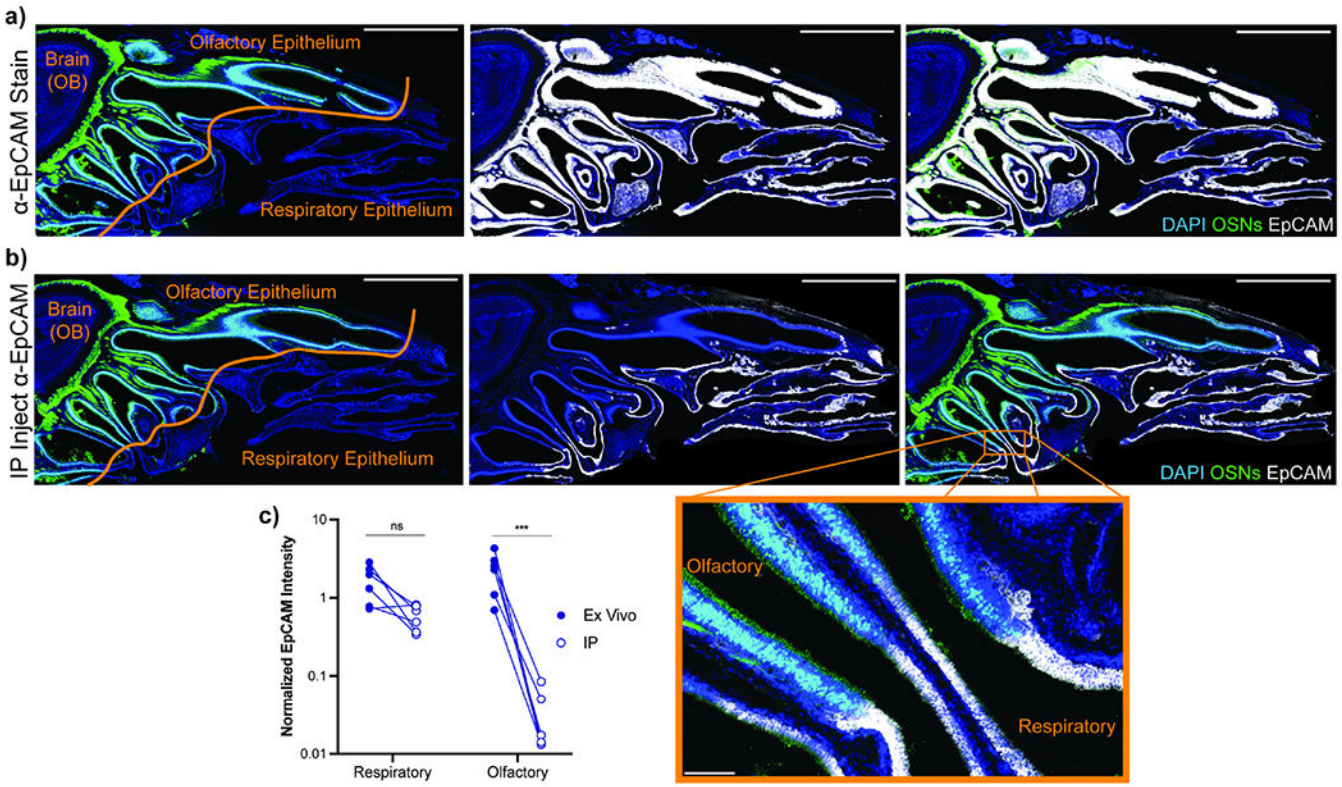

Figure 3 - Circulating Antibody Cannot Access Olfactory Epithelium

(a-b) 20 μg of anti-EpCAM antibody injected IP into OMP-GFP mice 12h before sacrifice. Serial sagittal head sections were prepared and either stained *ex vivo* with α-EpCAM primary antibody followed by DAPI and α-rat Alexa Fluor 647 **(a)** or stained only with α-rat Alexa Fluor 647 and DAPI **(b)** to reveal *in vivo* antibody distribution. Blue = DAPI, Green = OMP-GFP, White = α-EpCAM. Scale bar = 2 mm. Magnified image shows conversion of RE to OE, inset scale bar = 50 μm. **(c)** Quantification of α-EpCAM signal in a-b. Six sections across two mice analyzed for both groups. Olfactory regions defined by OMP-GFP expression, all other airway epithelial regions considered respiratory mucosa. Total EpCAM signal intensity following background correction was determined for each region and normalized to DAPI expression to account for variation in region size. Statistical significance determined by ratio paired t-test. ns (not significant) $P > 0.05$, *** $P < 0.001$. See also Figure S2.

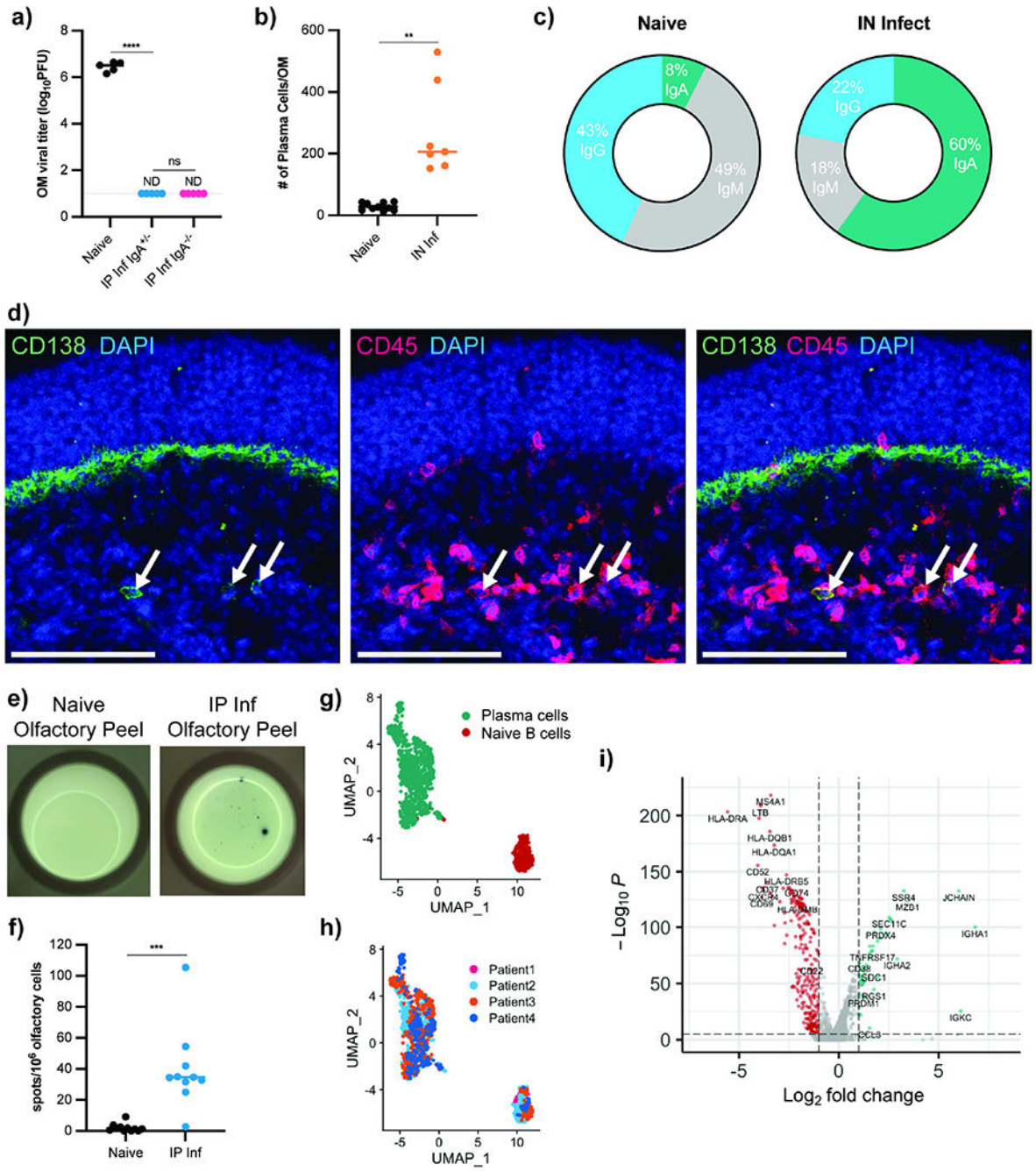

Figure 4 - Plasma Cells Exist in Mouse and Human Olfactory Mucosa

(a) OM VSV titers from $IgA^{-/-}$ (n = 5) and $IgA^{+/-}$ (n = 5) mice previously infected IN with VSV. At 35 dpi, mice rechallenged IN along with naïve $IgA^{-/-}$ mice (n = 5). OM VSV titers 48h after challenge. Data representative of two independent experiments. **(b-c)** Total OM plasma cells **(b)** and isotype proportions **(c)** from B6 mice infected with VSV IN (35 dpi, n = 7) and naïve mice (n = 9). Single cell OM suspensions gated on Live $CD45^{+}$ IN labeled-CD45.2+ and either IgG^{hi}, IgA^{hi}, or IgM^{hi}. Data pooled from two independent experiments. **(d)** Immunofluorescent staining of mouse OM 35d after IN VSV infection.

Arrows indicate $CD138^+$ $CD45^+$ plasma cells. Blue = DAPI, Red = CD45, Green = CD138. Scale bars = 100 μm. **(e-f)** ELISpot to detect VSV-specific antibody-secreting cells. OM peeled from the septum of naïve (n = 10) or d35 IP infected (n =10) mice. Representative image **(e)** and quantification **(f).** Data pooled from two independent experiments. **(g-i)** Published human OM single cell RNA-seq data from 4 healthy patients reanalyzed to identify antibody-producing cells. **(g)** UMAP dimensional reduction analysis of the subset of antibody-producing cells. Cluster analysis identified plasma cells (green) and naïve B cells (red). **(h)** Original patient identity of each sample. **(i)** Volcano plot showing significantly differentially expressed genes ($-\log_{10}$(adj P value) > 5, $\log_2$(FC) > 1) between plasma cells (green) and naïve B cells (red). Statistical significance in (a) determined using Ordinary One-Way ANOVA for multiple comparisons. Parametric unpaired t-test with Welch's correction used to assess statistical significance in (b) and (f). ND (not detected), ns (not significant), * $P < 0.05$, ** $P < 0.01$, *** $P < 0.001$, **** $P < 0.0001$. See also Figure S3.

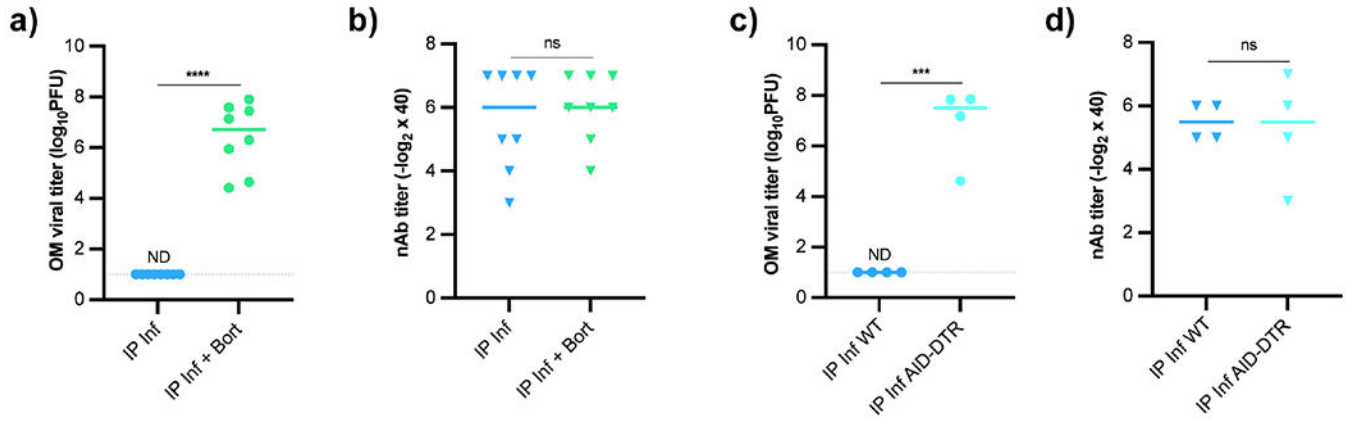

Figure 5 - Local Plasma Cells are Required to Protect the Olfactory Mucosa from Infection

(a-b) OM VSV titers **(a)** and plasma nAb titers **(b)** from mice IP infected and treated with bortezomib (n = 8) 21d after infection or untreated (n = 9). At 35 dpi, mice rechallenged with VSV IN. Data pooled from two independent experiments. **(c-d)** OM VSV titers **(c)** and plasma nAb titers **(d)** from $AID^{Cre/+}$ x iDTR mice (n = 4) or $AID^{+/+}$ control mice (n = 4) previously IP infected with VSV. Diphtheria toxin administered 21 and 22 dpi. Mice challenged IN with VSV at d35. Data representative of two independent experiments. For (a-d), parametric unpaired t-test used for significance. ND (not detected), ns (not significant), * $P < 0.05$, ** $P < 0.01$, *** $P < 0.001$, **** $P < 0.0001$. See also Figure S4.

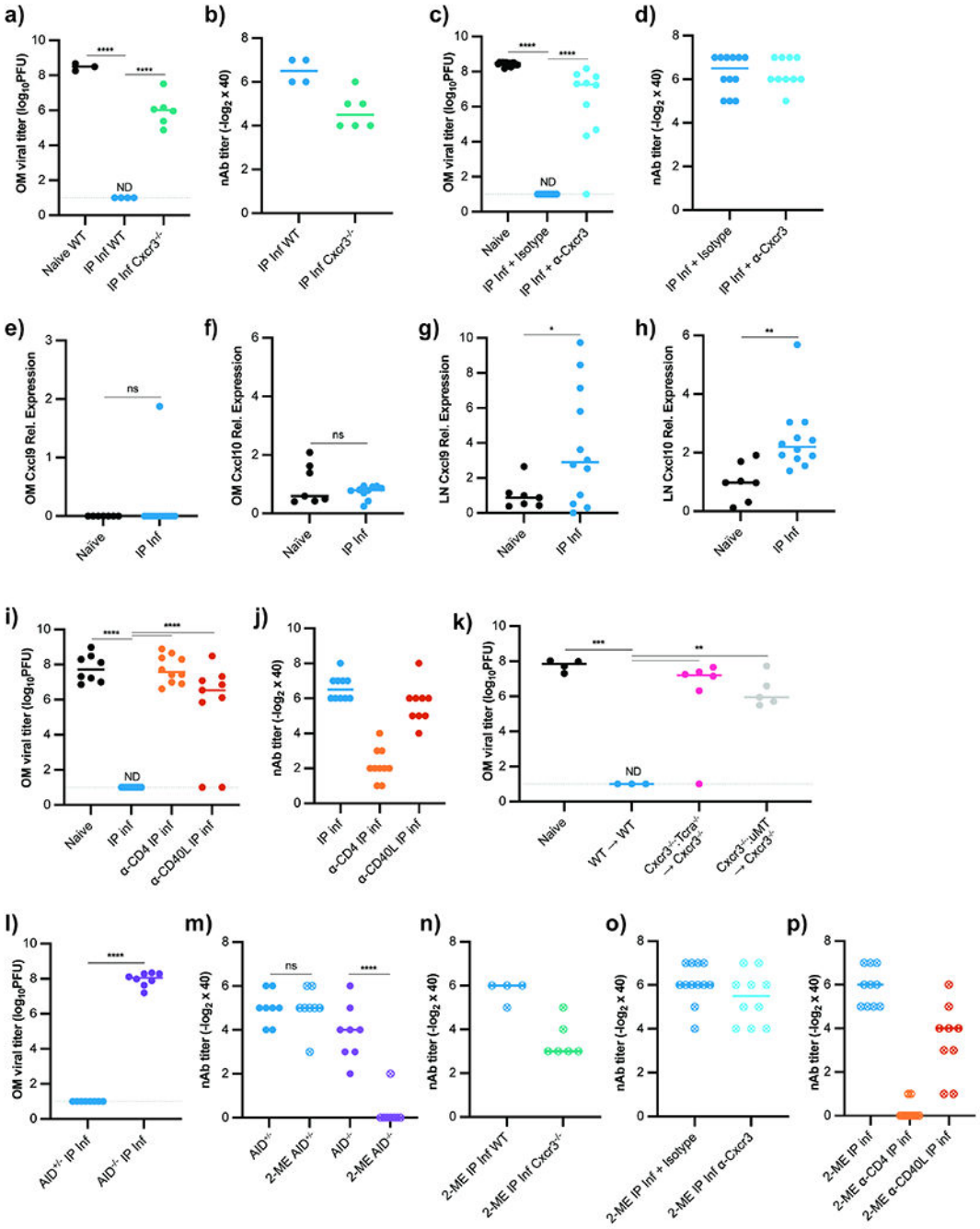

Figure 6 - Olfactory Plasma Cell Recruitment Depends on Cxcr3 and T cell Help

(a-b) OM VSV titers **(a)** and plasma nAb titers **(b)** from previously infected WT and $Cxcr3^{-/-}$ mice rechallenged IN with VSV. Experimental groups: naïve WT mice (n = 3), IP infected (21 dpi) WT mice (n = 4), and IP infected (21 dpi) $Cxcr3^{-/-}$ mice (n = 6). Data representative of two independent experiments. **(c-d)** OM VSV titers **(c)** and plasma nAb titers **(d)** from naïve (n =13), infected isotype control treated mice (n = 12), and infected α-CXCR3 mAb treated mice (n = 10). Antibody treatments given d1, 3, 5 after primary infection, and mice IN rechallenged 21 dpi. Data pooled from two independent experiments.

(e-h) qRT-PCR for *Cxcl9* and *Cxcl10* from naïve (n = 7) and VSV IP infected WT (n = 12) mice 4.5 dpi. **(e)** *Cxcl9* and **(f)** *Cxcl10* from OM. **(g)** *Cxcl9* and **(h)** *Cxcl10* from mediastinal LNs. Genes normalized to 18S mRNA and plotted as relative expression over mean from naïve group. Data pooled from two independent experiments. **(i-j)** OM VSV titers **(i)** and plasma nAb titers **(j)** from control and antibody-treated mice reinfected IN with VSV 21d after primary VSV IP infection. Experimental groups: naïve mice (n = 8), mice IP infected (n = 10), mice given α-CD4 depleting antibody 1d prior to IP infection (n = 10), and mice treated with α-CD40L blocking antibody 2d after IP infection (n = 9). Data pooled from two independent experiments. **(k)** OM viral titers from WT or $Cxcr3^{-/-}$ hosts irradiated and reconstituted with WT BM (n = 3), 70:30 $Tcr\alpha$:$Cxcr3^{-/-}$ BM (n = 6), or 70:30 μMT:$Cxcr3^{-/-}$ BM (n = 5). Mice IP infected with VSV 8 weeks after irradiation and rechallenged IN with VSV 21d later. **(l)** OM viral titers from IN rechallenged $AID^{-/-}$ (n = 8) or WT mice (n = 8), data pooled from two independent experiments. **(m-p)** Plasma nAb titers with 2-mercaptoethanol treatment for **(m)** $AID^{-/-}$ mice (from l), **(n)** $Cxcr3^{-/-}$ mice (from a, b), **(o)** α-Cxcr3 treated mice (from c, d), and **(p)** α-CD4 and α-CD40L treated mice (from g). For (a, c, i, k), statistical significance determined using Kruskal-Wallis One Way ANOVA for multiple comparisons. For (e-h, l), parametric unpaired t-test used for significance. In (m) statistical significance determined by ratio paired t-test. ND (not detected), ns (not significant), * $P < 0.05$, ** $P < 0.01$, *** $P < 0.001$, **** $P < 0.0001$. See also Figure S5.

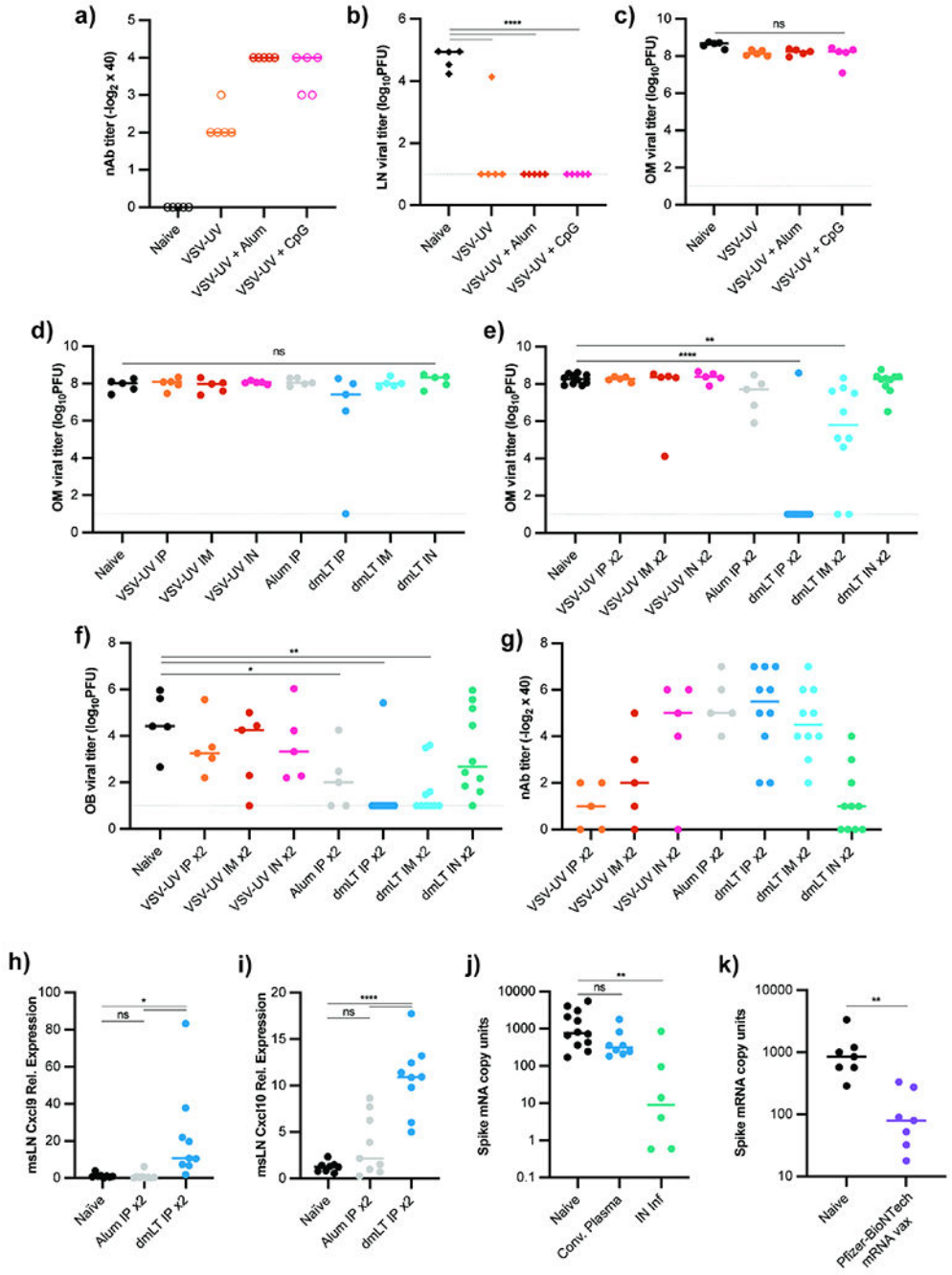

Figure 7 - A Mucosal Adjuvant, but not Conventional Adjuvants, Drives Olfactory Mucosa Protection

(a) nAb titers from mice immunized with UV-inactivated VSV combined with different adjuvants. Data representative of two independent experiments. Naïve (n = 5), VSV-UV only (n = 5), VSV-UV + alum (n = 5), and VSV-UV + CpG (n = 5) mice. **(b)** LN VSV titers from mice immunized as in (a) and challenged SC with VSV 21d after immunization. **(c)** OM VSV titers from mice in (a) IN challenged 21d after immunization. **(d)** OM VSV titers from mice immunized with VSV-UV alone or combined with Alum or dmLT 21d before IN

challenge. Immunization route (IP, IM, or IN) indicated for each group (n = 5 for all groups). **(e-g)** OM **(e)** and OB **(f)** VSV titers from mice immunized as in (d), but 21d following initial dose, an identical dose and route of immunogen administered 21d before VSV IN challenge. **(g)** Plasma nAb titers from mice in (e, f). n = 5 for all groups except naïve and all dmLT groups (n = 10). Data pooled across two independent experiments. **(h-i)** qRT-PCR for *Cxcl9* **(h)** and *Cxcl10* **(i)** from mice that received 2 IP immunizations with either VSV-UV + alum (n = 9) or VSV-UV + dmLT (n = 10) 21 days apart. Mediastinal LNs harvested 12h following second immunization. Data pooled from two independent experiments. Genes normalized to 18S mRNA and plotted as relative expression over mean from naïve group (n = 8). **(j)** OM VSV-SARS-CoV2 titers in naïve K18-hACE2 mice (n=11), K18-hACE2 mice infected IN 21d prior to rechallenge (n=6), or K18-hACE2 receiving convalescent plasma (n = 8) 12h prior to IN challenge. Viral titers quantified by normalizing Spike mRNA to 18S mRNA. Data pooled from two independent experiments. **(k)** OM viral titers from Naïve K18-hACE2 mice (n = 7) or K18-hACE2 mice (n = 7) given Pfizer-BioNTech Sars-CoV2 vaccine IM 21d prior to IN VSV-Sars-CoV-2 challenge. SARS-CoV-2 Spike mRNA normalized to 18S mRNA. Data pooled from two independent experiments. For (b-f, h-i), statistical significance determined using Ordinary One-Way ANOVA with multiple comparisons. In (j), Kruskal-Wallis One-Way ANOVA with multiple comparisons used for statistical significance. In (k), Kolmogorov-Smirnov unpaired t-test was used. ND (not detected), ns (not significant), * $P < 0.05$, ** $P < 0.01$, *** $P < 0.001$, **** $P < 0.0001$. See also Figure S6.

KEY RESOURCES TABLE

REAGENT or RESOURCE	SOURCE	IDENTIFIER
Antibodies		
α-mouse CD45.2 Clone 104 (Pac Blue); 1:10 dilution IN	Biolegend	Cat 109820
α-mouse CD45 Clone 30-F11 (BUV395); 1:500 dilution	BD	Cat 564279
α-mouse B220 Clone RA3-6B2 (BV-711); 1:500 dilution	Biolegend	Cat 103255
α-mouse IgG Poly4053 (APC); 1:250 dilution	Biolegend	Cat 405308
α-mouse IgA Clone C10-3 (FITC); 1:250 dilution	BD	Cat 559354
α-mouse IgM Clone RMM-1 (PE-Cy7); 1:250 dilution	Biolegend	Cat 406513
Zombie Viability UV Dye; 1:1000	Biolegend	Cat 423107
α-mouse EpCAM Clone G8.8	BioXCell	Cat BE0346
α-rat-AlexaFluor647	Jackson Immunoresearch	Code 712-605-153
α-mouse CXCR3 Clone CXCR3-173	BioXCell	Cat BE0249
α-mouse CD4 Clone GK1.5	BioXCell	Cat BE0003-1
α-mouse CD40L Clone Mr-1	BioXCell	Cat BE0017-1
α-mouse CD8 Clone YTS 169.4	BioXCell	Cat BE0117
α-mouse NK1.1 Clone PK136	BioXCell	Cat BE0036
Bacterial and virus strains		
VSV ovalbumin, serotype Indiana	(Kim et al., 1998)	N/A
VSV ovalbumin, serotype New Jersey	(Kim et al., 1998)	N/A
VSV-Sars-S-GFP	(Case et al., 2020)	SRA: SRR11878607
Influenza B/Malaysia/2506/2004 (Mal/04)	N/A	NCBI:txid464417
Mal/04-Cre	(Dumm et al., 2019)	N/A
Chemicals, peptides, and recombinant proteins		
VI10 anti-VSV mAb	(Kalinke et. al., 1996)	N/A
Bortezomib	Millipore	CAS 179324-69-7
Marizomib	Sigma	SKU SML1916
Imject Alum	ThermoFisher	Cat: 77161
CpG ODN 2395	Invivogen	Cat: tlrl-2395
dmLT (Enterotoxigenic *E. coli* Double Mutant Heat-Labile Toxoid)	BEI Resources	NR-51683
SARS-CoV-2 mRNA vaccine	Pfizer-BioNTech	N/A
Critical commercial assays		
QIAamp Viral RNA Isolation Kit	Qiagen	#52904
Express One-Step Superscript qRT-PCR Kit	ThermoFisher	#1178101
Deposited Data		
Previously published single-cell RNA sequencing data	(Durante et. al., 2020)	GEO accession code: GSE139522
Experimental models: Cell lines		
Monkey: Vero cells	ATCC	CCL-81
Monkey: Vero E6 cells	ATCC	CRL-1586

REAGENT or RESOURCE	SOURCE	IDENTIFIER
Canine: MDCK cells	ATCC	CCL-34
Experimental models: Organisms/strains		
Mouse: C57BL/6J (B6)	Jackson Laboratories	RRID:IMSR_JAX:000664
Mouse: B6.129(Cg)-*Gt(ROSA)26Sor*$^{tm4(ACTB-tdTomato,-EGFP)Luo}$/*J* (mT/mG)	Jackson Laboratories	RRID:IMSR_JAX:007676
Mouse: B6.*129P2-Cxcr3*^{tm1Dgen}/*J* (Cxcr3$^{-/-}$)	Jackson Laboratories	RRID:IMSR_JAX:005796
Mouse: B6.*129S2-Ighm*^{tm1Cgn}/*J* (μMT)	Jackson Laboratories	RRID:IMSR_JAX:002288
Mouse: B6;*129S2-Tcra*^{tm1Mom}/*J* (Tcra$^{-/-}$)	Jackson Laboratories	RRID:IMSR_JAX:002116
Mouse: B6.129P2-*Aicda*$^{tm1(cre)Mnz}$/J (AID$^{Cre/+}$, AID$^{-/-}$)	Jackson Laboratories	RRID:IMSR_JAX:007770
Mouse: C57BL/6-*Gt(ROSA)26Sor*$^{tm1(HBEGF)Awai}$/J (iDTR)	Jackson Laboratories	RRID:IMSR_JAX:007900
Mouse: B6.Cg-Tg(K18-ACE2)2Prlmn/J (K18)	Jackson Laboratories	RRID:IMSR_JAX:034860
Mouse: B6;129P2-*Omp*^{tm3Mom}/MomJ (OMP-GFP)	Jackson Laboratories	RRID:IMSR_JAX:00666
Oligonucleotides		
Cxcl9 FWD: AGGCACGATCCACTACAAATC (500 nM)	This paper	N/A
Cxcl9 REV: GCAGGTTTGATCTCCGTTCT (500 nM)	This paper	N/A
Cxcl9 Probe: /56-FAM/CCTCAAAGA/ZEN/ CCTCAAACAGTTTGCCC/3IABkFQ/ (200 nM)	This paper	N/A
Cxcl10 FWD: GGCCATAGGGAAGCTTGAAA (500 nM)	This paper	N/A
Cxcl10 REV: CAGACATCTCTGCTCATCATTCT (500 nM)	This paper	N/A
Cxcl10 Probe: /5SUN/TCCTGCCCA/ZEN/CGTGTTGAGATCATT/ 3IABkFQ/ (200 nM)	This paper	N/A
Eukaryotic 18s rRNA Endogenous Control	ThermoFisher	# CCU002NR
SARS CoV-2 S FWD: ACAGGCACAGGTGTTCTTAC (500 nM)	This paper	N/A
SARS CoV-2 S REV: GATCACGGACAGCATCAGTAG (500 nM)	This paper	N/A
SARS CoV-2 S Probe: /56-FAM/CTGCCTTTC/ZEN/ CAACAATTTGGCAGAGAC/3IABkFQ/	This paper	N/A
Software and algorithms		
Imaris v7.6.1	Bitplane	N/A
Flowjo v10.8.1	BD	N/A
R v4.0.3	R Project	N/A
Seurat v4.1.0	Satija Lab	N/A
Prism v9.1.2	GraphPad	N/A
Complete code for analysis of single-cell RNA sequencing data	This paper	DOI: 10.5281/ zenodo.7015296https://zenodo.org/ badge/latestdoi/474683647